

TDCOSMO

XIX. Measuring stellar velocity dispersion with sub-percent accuracy for cosmography

Shawn Knabel,¹ Pritom Mozumdar,¹ Anowar J. Shajib,^{2,3,*} Tommaso Treu,¹ Michele Cappellari,⁴ Chiara Spiniello⁴
Simon Birrer⁵

(Affiliations can be found after the references)

Received xxx, xxxx; accepted xxx, xxxx

ABSTRACT

Stellar velocity dispersion (σ) of massive elliptical galaxies is a key ingredient to breaking the mass-sheet degeneracy and obtaining precise and accurate cosmography from gravitational time delays. The relative uncertainty on the Hubble constant H_0 is double the relative error on σ . Therefore, time-delay cosmography imposes much more demanding requirements on the precision and accuracy of σ than galaxy studies. While precision can be achieved with an adequate signal-to-noise ratio (SNR), accuracy depends critically on factors such as elemental abundances and temperature of stellar templates, flux calibration, and wavelength ranges. We carry out a detailed study of the problem using multiple sets of galaxy spectra of massive elliptical galaxies with $\text{SNR} \sim 30\text{--}160 \text{ \AA}^{-1}$, and state-of-the-art empirical and semi-empirical stellar libraries and stellar population synthesis templates. We show that the choice of stellar library is generally the dominant source of residual systematic error. We propose a general recipe to mitigate and account for residual uncertainties. We show that sub-percent accuracy can be achieved on individual spectra with our data quality. Covariance between velocity dispersions measured for a sample of spectra can also be reduced to sub-percent levels. We recommend this recipe for all applications that require high precision and accurate stellar kinematics, and make all software publicly available to facilitate its implementation. This recipe will be used in future TDCOSMO collaboration papers.

Key words. cosmology: distance scale – gravitational lensing: strong – Galaxy: kinematics and dynamics – Galaxies: elliptical and lenticular, cD

1. Introduction

Stellar velocity dispersion (σ) has been a key observable for our understanding of massive elliptical galaxies for decades (Faber & Jackson 1976). Advances in spectroscopy, stellar populations and dynamical models have enabled the understanding of their internal structure, orbital anisotropy, mass-to-light ratio, and many other fundamental properties. The tight correlations between stellar velocity dispersion and other parameters are a testbed for any galaxy formation model (see review by Cappellari 2016).

In the past two decades, it has been shown that stellar velocity dispersion is particularly powerful in combination with strong gravitational lensing (e.g., Treu 2010, and references therein). As a purely dynamical probe, stellar velocity dispersion probes the full three-dimensional structure of galaxies and is insensitive to the mass-sheet degeneracy (Koopmans et al. 2003). Conversely, lensing probes the total projected mass (Dutton et al. 2011) and is insensitive to the mass anisotropy degeneracy (Mamon & Lokas 2005; Courteau et al. 2014).

For all these reasons, stellar velocity dispersion measurements have assumed a central role in the effort to infer cosmological parameters using gravitational time delays in galaxy-scale lenses, hereafter time delay cosmography (Suyu et al. 2010; Treu & Marshall 2016; Treu et al. 2022; Birrer et al. 2024). By constraining the mass distribution of the deflector (typically a massive elliptical galaxy) (Treu & Koopmans 2002) and by breaking the mass-sheet degeneracy, stellar velocity dispersions can, in principle, help achieve percent-level precision on H_0 , partic-

ularly when spatially resolved kinematics is available (Shajib et al. 2018; Yildirim et al. 2020; Birrer & Treu 2021).

However, in order for velocity dispersions to be a useful ingredient for time delay cosmography, precision and accuracy of better than 1% are needed, since the relative error on H_0 scales as double the error on stellar velocity dispersion: $\delta H_0 / H_0 = 2\delta\sigma / \sigma$ (e.g. Chen et al. 2021). Precision is relatively easy to achieve with modern instruments: spectra with current SNR and resolution are more than sufficient to obtain formal errors of order 1%. Furthermore, if errors are random and uncorrelated, it is sufficient to average multiple systems and/or measurements to obtain the desired precision. In contrast, potential systematic errors may bias individual measurements or introduce covariance between different galaxies – or within parts of the same galaxy – thus introducing an effective systematic noise floor, independent of the SNR or number of systems in the sample. Sources of systematics in stellar velocity dispersion measurements have been discussed for decades, and include instrumental resolution, bias due to insufficient signal-to-noise ratio, wavelength range, mismatch between templates and galaxy spectra in terms of elemental abundances and temperature, mismatch between template and galaxy continua, imperfect flux calibration, and interstellar absorption. Many excellent studies on this topic have been published in the past and inform the work presented here (e.g., Dressler 1984; Kelson et al. 2000; Treu et al. 2001; Barth et al. 2002; Spiniello et al. 2015; Spiniello et al. 2021a,b; Mehrgan et al. 2023; D’Ago et al. 2023).

In this paper, we revisit the issue of systematic errors in measured stellar velocity dispersion using multiple sets of galaxy spectra with $\text{SNR} \sim 30\text{--}160 \text{ \AA}^{-1}$ and state-of-the-art templates and

* NFHP Einstein Fellow

fitting code. Our goal is twofold: minimize systematic errors and quantify residual systematics in a principled, general, and reproducible way. In order to achieve our goal, we proceed as follows. In Section 2, we assemble a high-quality set of stellar and stellar population synthesis templates. The high-quality set of templates is made public for use by third parties. In Section 3, we present sets of spectra of elliptical galaxies at $z \sim 0.1 - 0.7$ observed with four different instruments (MUSE on VLT, KCWI on Keck, JWST-NIRSpec, SDSS; Bacon et al. 2010; Morrissey et al. 2018; Jakobsen et al. 2022). The SDSS spectra are included to compare with previous studies. In contrast, the three other sets of spectra are meant to represent the current state-of-the-art instruments used for stellar kinematics of lens galaxies.

In Section 4, we examine, quantify, and mitigate all known sources of systematics by running comprehensive sets of measurements. For all our fits, we use the well-tested and established code pPXF¹ (Cappellari & Emsellem 2004; Cappellari 2017, 2023). To guard against bugs in the utilization of pPXF and the construction of stellar libraries, SK and PM developed two independent pipelines. Several tests show that the two pipelines yield identical results when applied to the same data.

In Section 5, we propose a procedure to account for residual systematics by treating unconstrained choices (chiefly the choice of the stellar library) as nuisance parameters and marginalizing over them. The procedure can be used to estimate random and systematic errors as well as covariance between sets of measurements, e.g., spatial bins within a galaxy.

In Section 6, we show that by applying our procedure to high-quality spectra of elliptical galaxies, both systematic errors and covariance between independent galaxies or spatial bins can be contained to a sub-percent level. Our specific results only apply to the conditions described in this paper, in terms of instrumental setup, template libraries, and type of spectra under consideration. However, our procedure is entirely general and can be applied to any set of measurements to estimate the corresponding systematic noise floor. We recommend our recipe for all applications that require high precision and accurate stellar kinematics, and we make all software publicly available to facilitate its implementation. This recipe will be used in future TDCOSMO collaboration papers.

In Section 7, we summarize and discuss our results.

2. Stellar libraries and Single Stellar Population (SSP) models

In this section, we briefly describe the stellar libraries used in this work, referring to the original papers for more details (§ 2.1). We then describe our rigorous process to “clean” the libraries in Section 2.2. In Section 2.3, we compare the parameter space covered by the libraries relative to each other and before and after cleaning, as well as the spectra of the stars that are in common between the libraries.

2.1. Description of libraries

We consider two types of templates for the kinematic extraction: (i) individual stellar spectra and (ii) stellar-population synthesis models based on those stellar libraries. As empirical stellar libraries, we use three that are commonly employed in stellar kinematics

determination: Indo-US² (Valdes et al. 2004), MILES³ (Sánchez-Blázquez et al. 2006; Falcón-Barroso et al. 2011), and X-shooter Spectral Library (XSL)⁴ (Verro et al. 2022). Additionally, we include the sMILES stellar library, a semi-empirical library derived by modifying the MILES stellar spectra to represent different α element abundances (Knowles et al. 2021). This modification is meant to address template mismatch issues often encountered in the study of massive elliptical galaxies (Barth et al. 2002; Mehrgan et al. 2023). However, it is important to note that these models have known limitations, particularly in the blue part of the optical spectrum (Knowles et al. 2021, 2023). Therefore, our expectation is that they would not be sufficiently accurate for 1% kinematics. We include them for completeness.

As stellar population synthesis models, also known as single stellar populations (SSP), we use the E-MILES and sMILES, (hereafter E-MILES SSP and sMILES SSP, Vazdekis et al. 2010; Vazdekis et al. 2016; Knowles et al. 2023) and the SSP based on the XSL library (hereafter XSL SSP, Verro et al. 2022). While these models offer a physically motivated mix of stars, they lack the flexibility provided by individual stellar spectra. Therefore, they cannot reproduce the complexity of real star formation histories and chemical enrichment histories and are unlikely to be sufficient for sub-percent accuracy. However, they have been popular choices in the past. Therefore, we investigate them for completeness in order to determine how well they agree with the stellar libraries.

The Indo-US and MILES libraries have an approximately constant full width at half maximum (FWHM) kinematic resolution of 1.36 Å and 2.5 Å, respectively (Falcón-Barroso et al. 2011), which correspond to $\sigma_t \approx 43 \text{ km s}^{-1}$ and 80 km s^{-1} , respectively, at 4000 Å. For all MILES-based libraries (E-MILES, sMILES, etc.), we adopted 2.5 Å as the FWHM resolution of the templates. The kinematic resolution of the XSL templates is $\sigma_t \approx 13 \text{ km s}^{-1}$ at the UVB region (3000–5560 Å), 11 km s^{-1} at the VIS region (5330–10200 Å), and 16 km s^{-1} at the NIR region (9940–24800 Å). We refer the reader to the original papers for a full description of the libraries.

2.2. Cleaning the stellar libraries

The full stellar libraries contain spectra of variable quality, including some with defects, incomplete data, incomplete calibration, or low SNR. Indeed, when using stellar spectra to construct stellar population synthesis models, the original papers apply quality cuts (Vazdekis et al. 2016; Verro et al. 2022).

In order to obtain “clean” spectral libraries, we took a series of steps. First, we eliminated all the spectra that were flagged by the original teams as faulty. For example, for XSL, the template FITS file headers contain keywords that indicate the applied corrections and quality flags, and some of the spectra were flagged as “peculiar”, “abnormal”, “zero” (see, e.g., Tables B.1 and C.1 of Verro et al. 2022). In addition, some spectra have not been corrected for slit losses. We eliminated from XSL all spectra listed in the aforementioned Table C.1 and all that were corrected for slit loss. Whenever possible we contacted the authors of the library to reproduce the selection applied to their construction of the stellar population synthesis models.

² <https://noirlab.edu/science/observing-noirlab/observing-kitt-peak/telescope-and-instrument-documentation/cflib>

³ <https://miles.iac.es/>

⁴ <http://xsl.u-strasbg.fr/>

¹ <https://pypi.org/project/ppxf/>

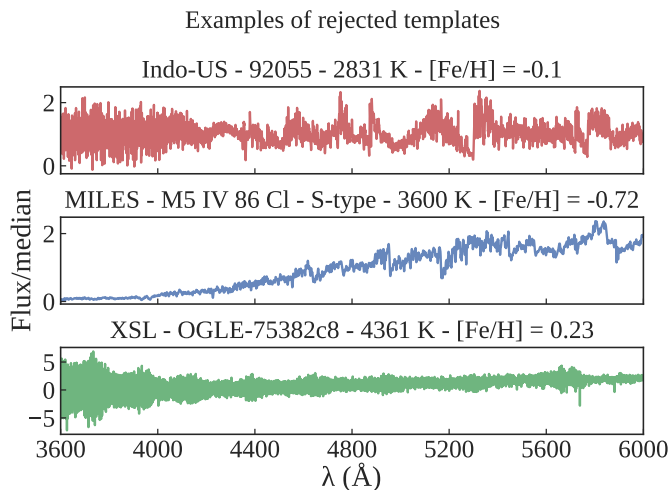


Fig. 1. Example of rejected templates from each of the three stellar libraries. For each spectrum, we state the library name, object name, T_{eff} , and metallicity above the respective panel. All three templates were removed because they were too noisy in the wavelength region of interest.

Second, we eliminated all the spectra with incomplete stellar parameters, especially temperature T_{eff} and metallicity Fe/H . For MILES and XSL, they represent a small fraction (1-2%) of the total number of stars, while for Indo-US, they are a larger fraction (20%). In almost all cases, they are faulty spectra (e.g., missing part of the spectral range, very noisy, or with obvious defects). We note that many of the spectra flagged by the authors of the MILES and XSL libraries are also missing T_{eff} and Fe/H . These two initial steps remove between 20-30% of the initial spectra for all three libraries. For reference, the Indo-US library has been used in the most recent versions of the SDSS kinematic pipeline (Bolton et al. 2008, and Bolton, A.S. private communication). However, to our knowledge, no cleaning was applied.

Third, we visually inspected all the individual spectra to identify defects or anomalies. Although, in general, the quality of the spectra is excellent, in very few cases, there were substantial anomalies (see Table 1 and Figure 1). The spectra were flagged for the following anomalies:

1. Improper flux calibration at the edges and near the dichroic. These spectra were kept in the clean libraries. However, we recommend avoiding/masking the regions near the edge and near the dichroic when performing the fits.
2. Improper correction of telluric absorption. These spectra were kept in the clean libraries. However, we recommend masking out the regions corresponding to the telluric A and B bands for high-accuracy work.
3. Some spectra, more commonly from the Indo-US library, have localized gaps that can extend for 100s or 1000s of Å. We do not exclude them from the clean library, but we recommend excluding them if the gaps overlap with the fitted range.
4. Some spectra show clear emission lines, which could be due to the contamination by other astronomical targets along the line of sight. Those have been removed from the clean library, as they modify the stellar absorption lines with infilling.
5. Some spectra are much noisier than the galaxy spectra we consider in this work (see examples in Figure 1). They have been removed from the clean library as they are too noisy for precision work.

Table 1. Number of stars in stellar libraries. The first row lists the initial number of stars in each library. The second one is how many are left after quality cuts applied by the authors of the libraries in the construction of SPS models. The third row removes stars that do not have consistent estimates of T_{eff} and Fe/H (usually poor-quality spectra). The fourth row lists the number of stars that are left after a final round of visual inspections, as described in the main text.

Step	# MILES	# XSL	# Indo-US
Initial	985	830	1273
After library authors' cuts	801	530	1273
With T_{eff} and Fe/H	790	522	1006
After visual Inspection	789	496	992

6. A very small number of spectra have clear defects, possibly resulting from imperfect reduction or calibration (e.g., there is one spectrum for which the flux of the extinction corrected spectrum is below that of the original one in the red). Those have been excluded from the clean library.

After the cleaning procedure, the stellar libraries consist of 789, 496, and 992 stars, as summarized in Table 1. The list of stars in the “clean” stellar libraries will be made available in electronic format through GitHub https://github.com/TDCOSMO/KINEMATICS_METHODS after the acceptance of this manuscript.

2.3. Comparing parameter space and common stellar spectra

In order to get an unbiased estimate of the stellar velocity dispersion, it is important to use stellar libraries that span the range of temperature and metallicity expected to dominate the spectra of massive elliptical galaxies. The distribution of these two parameters for the stellar libraries before and after cleaning is unaffected, demonstrating that the quality cuts do not exclude important parts of the parameter space and remain representative of the original libraries.

We also tested whether the distribution of the stellar libraries within the parameter space affects the outcome. Figure 2 shows that with spectra of sufficient quality and wavelength coverage, pPXF is able to recover the correct stellar velocity dispersion and stellar mix, irrespective of the distribution in temperature and metallicity of the stellar spectra within the library.

For the clean stars in common between the libraries, we compared the spectra visually and in terms of their ratio. Some examples are shown in Figure 3. Overall, the comparison is excellent, even though there are some instances in which the ratio differs significantly from one, indicating systematic residuals in the flux calibration and reddening corrections. These differences underscore the importance of having additive and multiplicative polynomial continuum components in the kinematic fits, as discussed below.

3. Galaxy samples

Our goal is to investigate systematic errors in the measurement of stellar kinematics of massive elliptical galaxies, which comprise the vast majority of deflectors in galaxy-scale strong gravitational lenses. To be sensitive to percent level effects in the systematic errors and covariance, we need spectra with sufficiently high SNR of galaxies that are gravitational lenses – or that are in

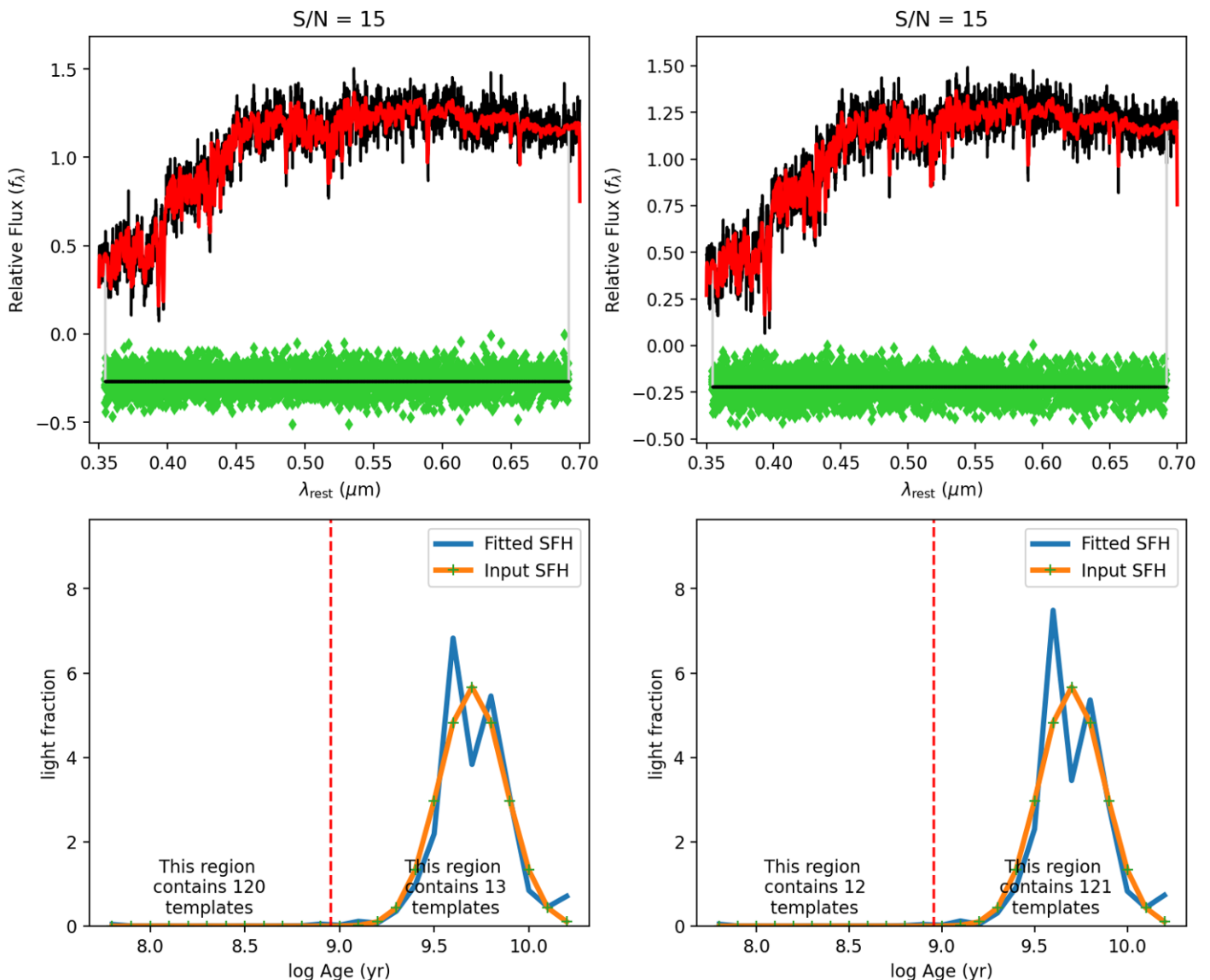


Fig. 2. Test of the ability to recover the correct mix of templates, irrespective of the prior density in temperature and metallicity space. The red dashed lines in the bottom-panel plots distinguish the temperature and metallicity spaces. The simulated spectrum is based on a mix of templates from the MILES library and then fits with a wider library of stellar templates. If the correct templates are present in the library, there is enough information to select the correct ones, even if they represent a small fraction of the library.

the appropriate redshift and luminosity range to represent strong gravitational lenses.

Our first sample is a set of massive elliptical galaxies observed with the MUSE spectrograph (Bacon et al. 2010) on VLT, described in Section 3.1. Our second sample is a set of gravitational lens galaxies observed with KCWI on the Keck Telescope, described in Section 3.2. We also consider the high-quality spectrum of the lens galaxy RXJ1131–1231 observed with JWST-NIRSpec (Jakobsen et al. 2022) (Section 3.3). Even though it is only one galaxy, there are many spectral bins within the galaxy, and thus, one can observe the covariance between the spectra. Furthermore, NIRSpec covers the rest frame CaT region, which is difficult to reach from the ground at our redshifts of interest. Thus, NIRSpec allows us to quantify systematics in a different wavelength region from MUSE and KCWI. Finally, we also study a sample of spectra taken by the Sloan collaboration (Section 3.4). Those generally have a much lower SNR than the other spectra considered here. However, they have been broadly used in the literature. Therefore, we think it might be of interest

to the reader to see how our considerations apply to the SDSS dataset.

Throughout this section, we use a SNR metric to compare the quality of data across different instruments. Our chosen metric is the average SNR per \AA , measured in the rest frame wavelength interval of 4000–4500 \AA (chosen to be redward of the 4000 \AA break, where the SNR per pixel is relatively uniform). This is obtained by averaging the signal-to-noise per pixel, divided by the square root of the number of \AA per pixel. This metric is not applicable to our JWST data, owing to the spectral range covered. For that dataset, we modify the wavelength range to 8303–8838 \AA . For comparison across different wavelength ranges and surveys, it is also interesting to consider the SNR per 70 km s^{-1} interval (the SDSS pixel resolution). At our fiducial pivot point 4250 \AA , 70 km s^{-1} is almost exactly 1 \AA .

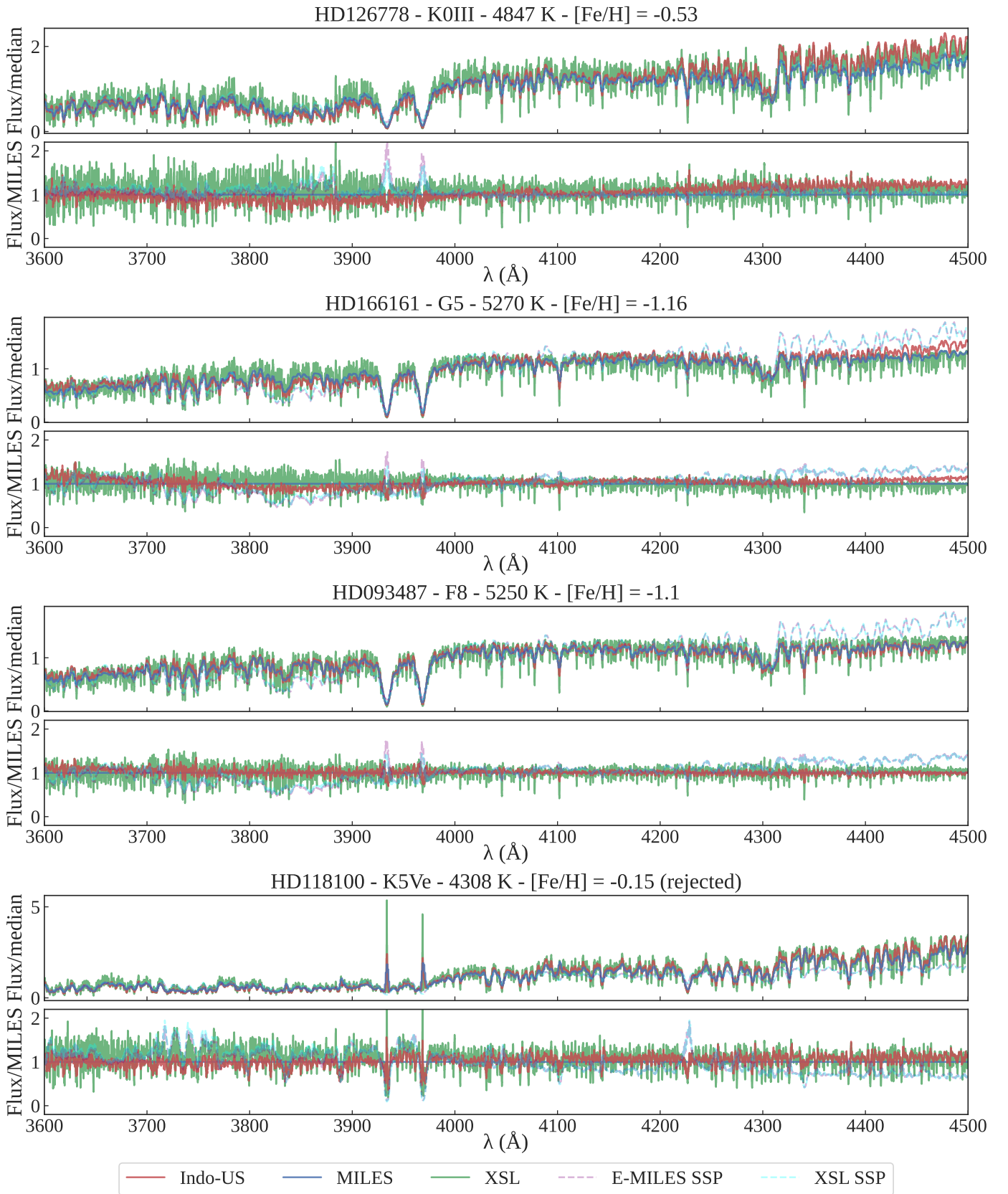


Fig. 3. Example spectra of stars in common between the three libraries. For each example, the spectra are shown in the top panel of the two, and ratios with respect to the MILES spectrum are shown in the bottom one. SSP spectra with solar metallicity and 10 Gyr age are also shown for comparison. The fourth template shown (HD118100) was removed from all three clean libraries, owing to the strong emission lines in the CaHK absorption features. It was removed from MILES by author selection and was flagged independently by visual inspection in the other two libraries.

3.1. VLT-MUSE

The Multi-Unit Spectroscopic Explorer (MUSE) is an integral-field spectrograph situated at the Very Large Telescope (VLT) of the European Southern Observatory (ESO). It provides a spatial sampling of $0.2''$ across a $1^{\prime 2}$ field-of-view (FOV) in its wide-field mode (Bacon et al. 2010). It operates within a wavelength range of $\lambda = 4650\text{--}9300 \text{ \AA}$ with a reciprocal dispersion of 1.25 \AA per pixel. The FWHM spectral resolution is approximately 2.5 \AA around 5000 \AA which corresponds to an instrumental dispersion of 65 km s^{-1} . The galaxies in the original MUSE sample are selected using the integral field unit (IFU) datacubes from the ESO Science Archive under the MUSE-DEEP program⁵ which consolidates observations from single or multiple MUSE programs at specific sky locations into a single IFU datacube, achieving very high effective exposure times. The selection criteria, data extraction process, and other relevant information about the sample, such as galaxy ID and the galaxy cluster or field to which it belongs, ESO archive ID of the datacube, program IDs of the observations used to create the datacube, effective exposure, etc., are described in Mozumdar et al. (2025, in prep; hereafter M25). From the parent sample of M25, we first select a subsample of 140 galaxies that contain data within our adopted restframe wavelength range of $3600\text{--}4500 \text{ \AA}$ with $\text{SNR} > 30 \text{ \AA}^{-1}$. The central spectra of these galaxies were visually inspected to ensure that no reduction artifacts were present. A handful of spectra were removed due to reduction artifacts, poor sky subtraction, and the presence of strong emission lines. Finally, a velocity dispersion cut of $\sigma_v > 140 \text{ km s}^{-1}$ was applied to the sample. The reason for this cut is described in Section 4.1. In total, the final sample consists of 85 galaxies with an average integrated SNR of 60 \AA^{-1} . The redshift range of this sample is $0.29\text{--}0.67$. Some examples of the central spectra are shown in Figure 4.

3.2. Keck-KCWI

Fourteen of the Sloan Lens ACS Survey (SLACS) gravitational lenses (Bolton et al. 2006, 2008) were observed with KCWI on Keck, with the goal of measuring spatially resolved stellar kinematics. The data are fully described by Knabel et al. (2024). The data are collected in the wavelength range $3500\text{--}5600 \text{ \AA}$ in a $8.4'' \times 20.4''$ field of view, and the spectral resolution of $R \sim 3600$ corresponds to an instrumental dispersion $\sigma_{\text{inst}} = 35 \text{ km s}^{-1}$. The reciprocal dispersion is 0.5 \AA per pixel. The redshift range of the sample is $0.15\text{--}0.35$. In order to attain a high SNR and avoid contamination from the lensed background source, we integrate the datacube within a circular radius of $1''$ centered on the center of the foreground deflector galaxy. For most of our studies and unless otherwise specified, we use these $1''$ -integrated spectra. The average SNR of the sample is 160 \AA^{-1} within this radius. For comparison with SDSS spectra of these objects, we also extract spectra from the KCWI datacube integrated within the SDSS aperture-radius of $1.5''$. These spectra are shown in Figure 5 together with the corresponding SDSS spectra for comparison. We use these spectra exclusively for comparison with SDSS. We note that the SDSS spectra for this subsample of objects have insufficient SNR for our purposes and, therefore, will not be used in the overall analysis. We will, however, use a set of higher SNR spectra from SDSS, as described below.

3.3. JWST/NIRSpec

The gravitational lens RXJ1131–1231 was observed by JWST/NIRSpec in IFS mode (Böker et al. 2022) during Cycle 1 (Program 1794; PI Suyu, Co-PI Treu). The data analysis and processing are fully described by Shajib et al. (2025; in prep). We constructed the reduced datacube with a spaxel size of $0''.1$. The redshift of the lens is $z = 0.295$. The white-light image of the NIRSpec datacube and one example spectrum is shown in Figure 6.

We take 21 single spaxels within the central $0''.5 \times 0''.5$ region, excluding the four at the corners, of the lens galaxy (illustrated in Figure 6), over which we average our test results. We restrict the bins within the central region of the lens galaxy to minimize contamination from the background quasar and its host galaxy in the spectra adopted for the test. Additionally, we select a wavelength range ($8303\text{--}8838 \text{ \AA}$) sufficiently encompassing the Ca II triplet lines. This region also includes the H- α broad emission + [N II] lines from the quasar plus host galaxy appearing slightly blueward of the Ca II triplet and the [S II] lines from the host in between the two prominent Ca II lines at $\sim 8600 \text{ \AA}$. We model all these lines from the quasar and its host with additional kinematic components in our fit (for details, see Shajib et al., 2025, in preparation). However, for the tests performed in this paper, we only focus on the extracted kinematics from the lens galaxy’s Ca II triplet features.

We remove some spectra from the Indo-US and XSL stellar template libraries that have NaN values or coverage gaps within the fitted wavelength range, leaving us with 609 and 489 templates in them, respectively. We do not include the MILES stellar template library for the tests performed on the NIRSpec data as it does not cover the Ca II triplet’s wavelength region.

When extracting kinematics from the IFU data, it is standard practice in the literature (e.g., Westfall et al. 2019; Shajib et al. 2023) to first synthesize a single global template⁶. This single global template is obtained from the best-fit weighted combination of the whole template library when fitting to the spectra summed from multiple central spaxels or bins, which has a considerably larger SNR. After that, all the individual bins are fit using this single global template. This approach reduces bin-to-bin scatter in the extracted kinematic map for a single galaxy. The creation of a global template from a central region of the galaxy is included as an additional step to the methodology described in the previous section. We find that this additional step indeed reduces bin-to-bin scatter and, thus, in turn, the systematic scatter between the template libraries. Although this is helpful in reducing systematic scatter for the adopted case of NIRSpec spectra, this step may not be necessary for cases with a much higher SNR per spatial bin, where contamination from quasar or host galaxy lines can be robustly differentiated, unlike the specific case presented in this paper.

3.4. SDSS

For reference and comparison, we also consider SDSS spectra of a sample of galaxies that were identified by Bolton et al. (2008); Shu et al. (2015) as potential gravitational lenses. Targets were then selected from this list for follow-up with the Hubble Space Telescope, and the confirmed lenses represent the SLACS (Bolton et al. 2008) and “SLACS for the masses” (Shu

⁶ If the spatial extent is sufficient to span population gradients – a set of templates in radial annuli (Knabel et al. 2024). This is not necessary in this case, given that aperture corresponds to just $\sim 1 \text{ kpc}$.

⁵ <https://doi.org/10.18727/archive/42>

Example of central spectra for MUSE galaxies and pPXF fit

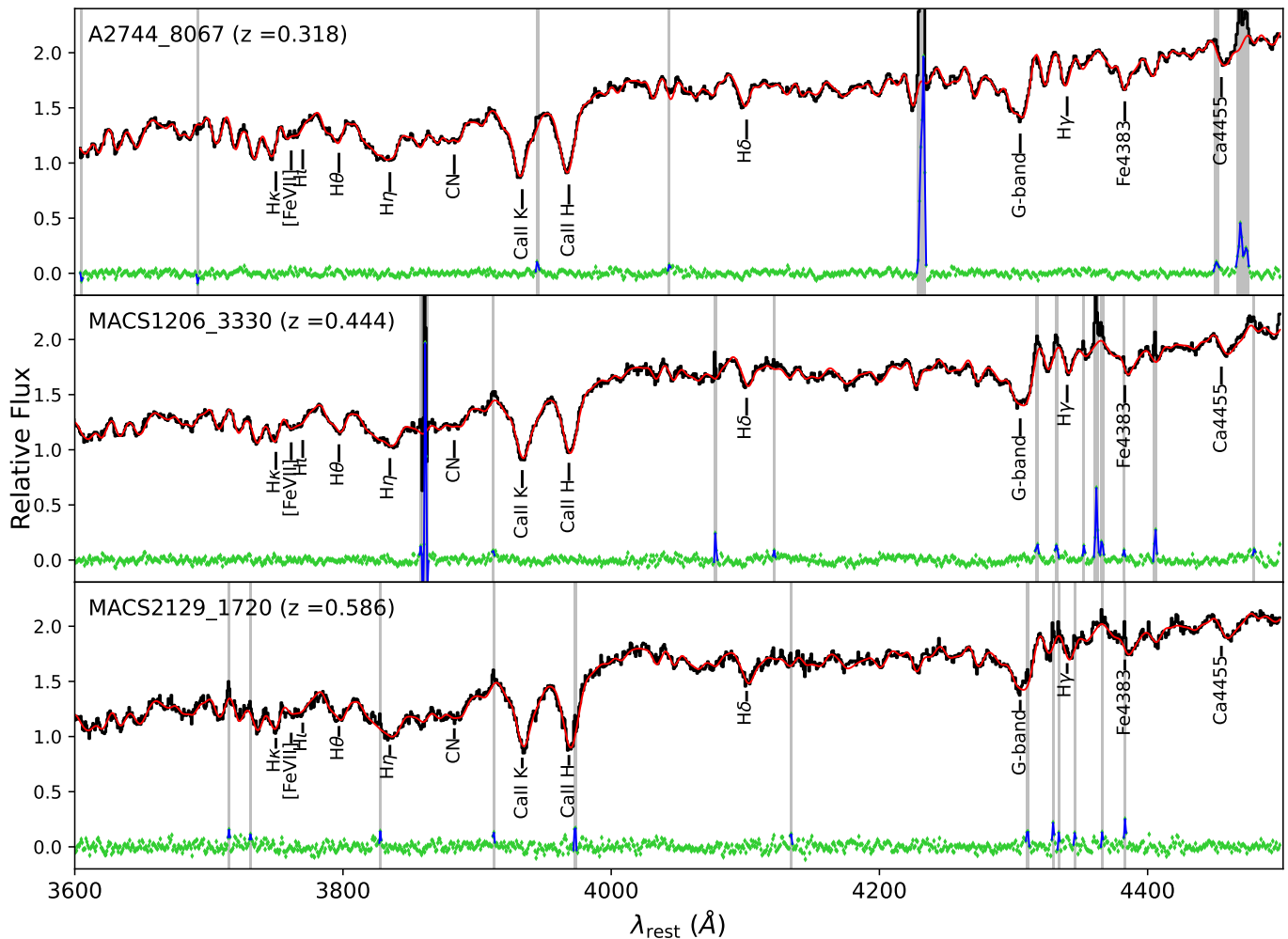


Fig. 4. Central spectra of three galaxies at different redshift from the MUSE sample. In each panel, the black line is the observed spectrum, and the red line is the best-fit model from pPXF. The gray regions mark the excluded wavelength range from fitting, and the green markers are residuals between data and the fitted model at each wavelength. The blue pixels, generally emission lines or sky residuals, have been excluded by sigma-clipping.

et al. 2015) lenses. Multiple velocity dispersion measurements are available for this sample from the early SDSS releases, the SLACS papers themselves, and the most recent data release, DR17 (Abdurro'uf et al. 2022). We refer to Knabel et al. (2024) for a detailed comparison between the KCWI and SDSS spectra. In general, the SDSS spectra have much lower SNR than required for the present analysis, as shown in Figure 5. However, 50 of them have $\text{SNR} > 15 \text{ \AA}^{-1}$. We present results for those here. An example of this set of relatively high SNR SDSS spectra is shown in Figure 7. This subsample of 50 SLACS lens candidates spans a lower redshift range than the KCWI sample ($z \sim 0.04 - 0.15$) with an average $\text{SNR} \sim 19 \text{ \AA}^{-1}$.

4. Testing for systematics

In this section, we describe a number of systematic tests conducted on our galaxy samples. As we will see, the dominant source of systematic errors turns out to be the choice of stellar templates, provided that reasonable choices are made for wavelength range and continuum polynomials. We first discuss sys-

tematic errors associated with the spectral resolution of the templates in Section 4.1. Then we discuss continuum polynomials (Section 4.2), cleaning templates (Section 4.3), choice of templates (Section 4.4), and wavelength range (Section 4.5).

4.1. Spectral resolution of the templates

In practice, the stellar velocity dispersion σ is inferred by comparing the data to a template, initially broadened to match the spectral resolution of the instrumental setup, to find the additional broadening imposed by the stellar kinematics.

Under a Gaussian approximation, the instrumental resolution of the spectrograph used to observe the template σ_t , and that used to observe the galaxy spectrum σ_s , are related to the total smoothing of the observed spectrum σ_o and the astrophysical stellar velocity dispersion σ by the equation:

$$\sigma^2 = \sigma_o^2 - \sigma_s^2 - \sigma_t^2 \quad (1)$$

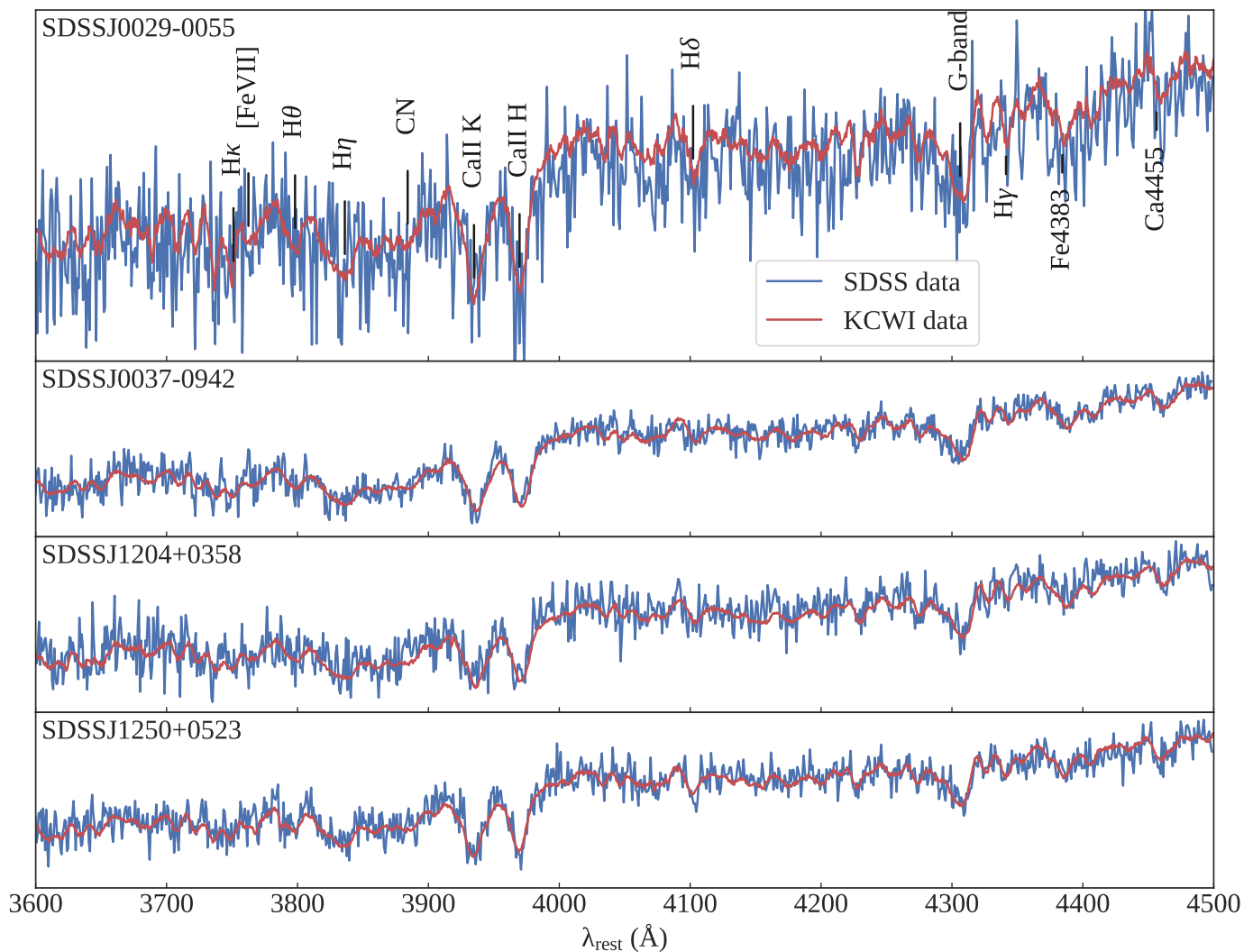


Fig. 5. Comparison between the KCWI (red) and SDSS (blue) spectra of the same objects in the wavelength range used for the KCWI fit. The KCWI spectra shown here are integrated over spaxels within a radius of $1.5''$, the same size as the SDSS fiber. SDSS spectra (blue) shown here have $\text{SNR} < 15 \text{ \AA}^{-1}$.

For small errors in the characterization of σ_s and σ_t , it is easy to show – by expansion to leading order – that the relative variations of the astrophysical velocity dispersion and the instrumental and template resolution measurements are related by the following equations. The relative variation in the astrophysical dispersion, at fixed σ_o and σ_s is:

$$\frac{\delta\sigma}{\sigma} \approx \frac{\delta\sigma_t}{\sigma_t} \left(\frac{\sigma_t}{\sigma} \right)^2, \quad (2)$$

While the relative variation at fixed σ_o and σ_t is:

$$\frac{\delta\sigma}{\sigma} \approx -\frac{\delta\sigma_s}{\sigma_s} \left(\frac{\sigma_s}{\sigma} \right)^2, \quad (3)$$

These variations are generally sub-percent. For example, even for a 10% error in the determination of an instrumental resolution of 50 km s^{-1} , the corresponding error on a velocity dispersion of 250 km s^{-1} is 0.4%. If they are random, e.g., stemming from instabilities of the spectral configuration of slit-filling effects in variable seeing, they will average out for a sample. If they are not random, one should ensure that they are below the noise floor required by the measurement.

For example, the MILES library has a resolution of approximately $\sigma_t \sim 80 \text{ km s}^{-1}$ at 4000 \AA , so if the goal is 1% errors on σ – assuming that the error on σ_t is 3% (Falc3n-Barroso et al. 2011) – according to Eq 2 it should not be used for stellar velocity dispersions below 140 km s^{-1} . In contrast, if the goal is 5%, MILES can be used down to 60 km s^{-1} . Since the goal of this paper is 1% we discard galaxies for which the higher resolution libraries (e.g. XSL) give velocity dispersions below 140 km s^{-1} , because MILES would not meet our accuracy standards for this paper and therefore we could not carry out the comparison between libraries.

4.2. Continuum/flux calibration Polynomials

The fitting code pPXF uses additive and multiplicative polynomials to account for mismatches between the templates and the galaxy spectra. Additive polynomials can represent light from non-stellar sources (e.g., an active nucleus), imperfect sky subtraction, or variations in continuum line strength to reduce template mismatch. Multiplicative polynomials can account for improper flux calibration due to slit losses or differential atmospheric dispersion.

NIRSpec white-light image

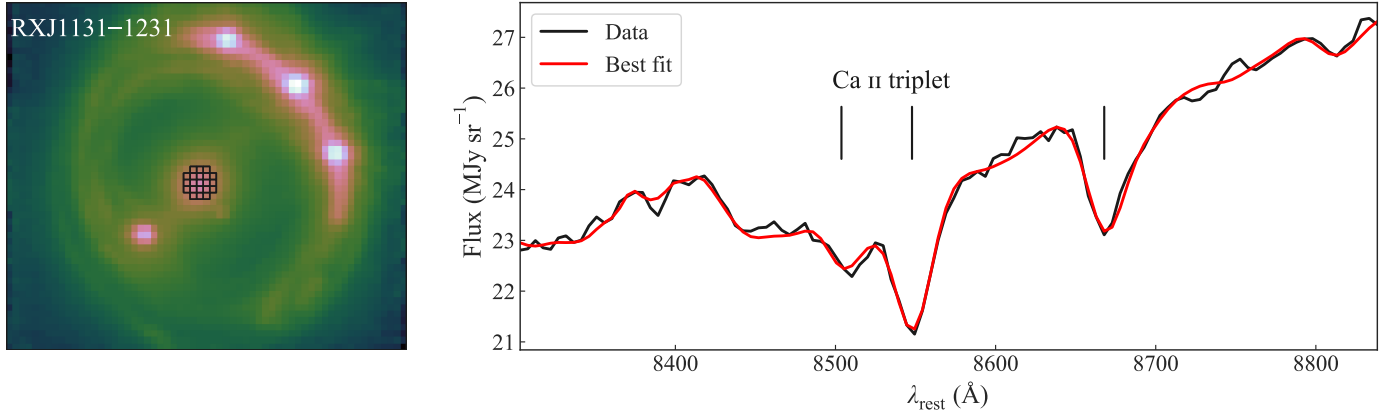


Fig. 6. JWST/NIRSpec observations of the lens galaxy RXJ1131–1231. **Left:** White-light image from the NIRSpec datacube. The 21 spaxels at the center of the lens galaxy, over which we average our test results, are traced with black squares. **Right:** The spectrum (black) from the central spaxel and the best fit (red) from pPXF using the “clean” Indo-US library. The Ca II triplets are marked with vertical lines.

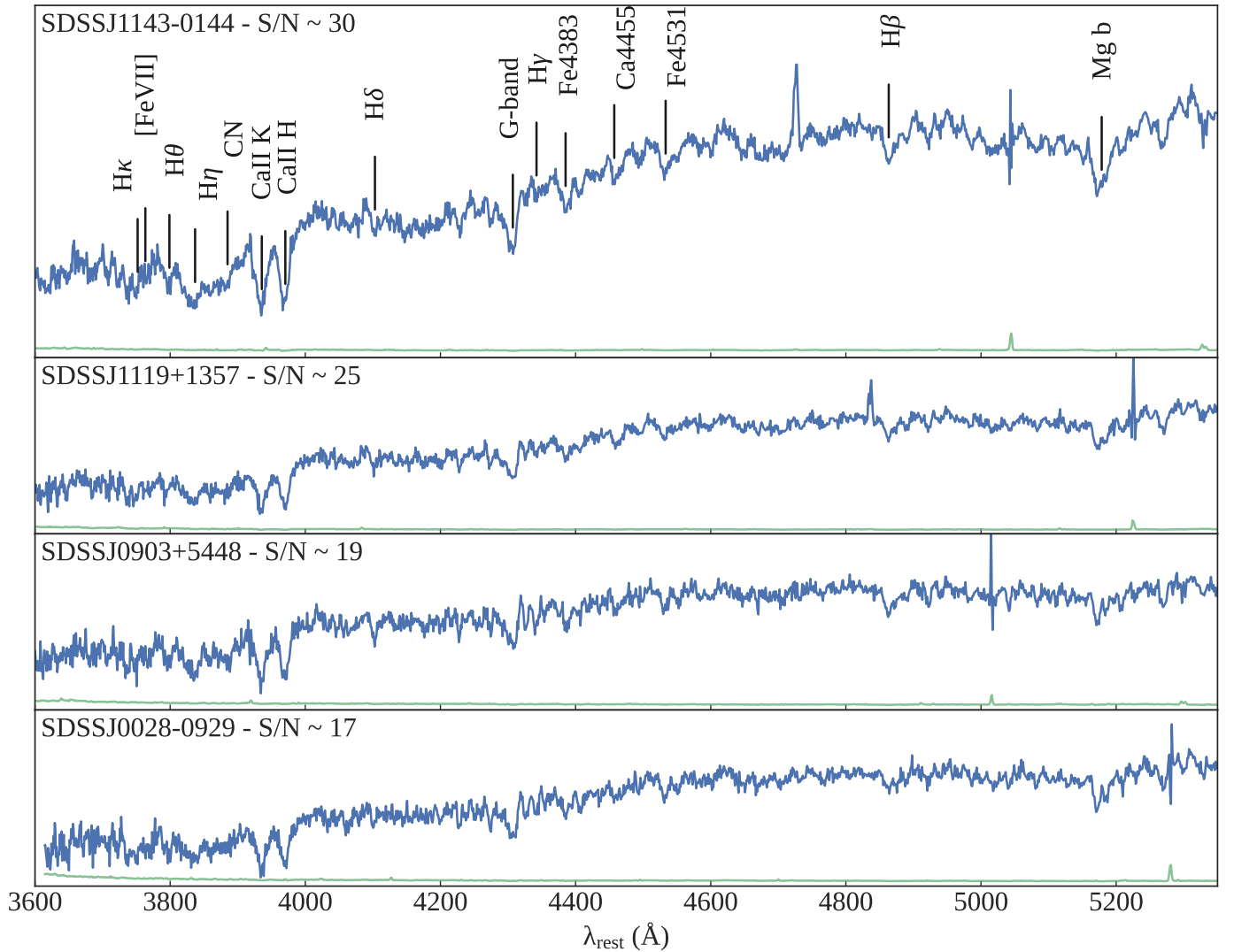


Fig. 7. Examples of SDSS spectra with $\text{SNR} > 15 \text{ \AA}^{-1}$, which is needed to measure kinematic extraction at the level of precision and accuracy we require in this study. The wavelength range shown is the range for fits involving the SDSS data. We take this range instead of using the entire SDSS spectrum because fits with XSL templates that cross the UVB-VIS dichroic above 5450 \AA are unreliable.

Additive polynomials are less computationally expensive than multiplicative ones and are often preferred for large datasets. However, the computational cost of multiplicative polynomials is still manageable for the sample described here, taking just a few minutes per galaxy. Our extensive tests show that there is usually a “sweet spot” in polynomial orders, where the results from the fit are very stable with respect to specific choices of templates or wavelength ranges. Choosing significantly lower or higher orders can result in significant discrepancies between the results. Therefore, we recommend running a grid of polynomial orders to identify the most appropriate ones for a specific dataset, depending on the wavelength range and accuracy of the spectrophotometric calibration (see, e.g., D’Ago et al. 2023, for a similar strategy).

In practice, we find that additive polynomials of order 6 (but also 5 or 7) and multiplicative polynomials of order 2 (but also 1 or 3) are appropriate for the adopted wavelength range (described in Section 4.5) for our MUSE/KCWI/SDSS datasets. For JWST-NIRSpec, we adopt an additive polynomial order of $n = 1$ and a multiplicative polynomial order of $m = 0$, owing to the shorter wavelength range and flatter overall continuum. As we will show in the next section, the residual systematic uncertainty associated with polynomial order choice is at the level of 0.2–0.5% for the datasets considered here.

4.3. Cleaning the libraries

The effect of cleaning the libraries is significant. Flawed template spectra can cause a variety of issues with the resulting model fit. For example, in the stellar spectrum in the lowest panel of Figure 3, the emission lines in the centers of the CaHK absorption features could artificially broaden and reshape the line profiles in combination with other stellar templates used in the fit. In Figure 8, we show the ratio of velocity dispersion measurements of the MUSE sample using ‘full’⁷ and ‘clean’ XSL, MILES, and Indo-US libraries (the results for the other samples are similar). We see that the effect is of order percent on average for MILES and Indo-US, but it is significantly larger for XSL. In some cases, the differences can be several percent, up to 5% or more. It is thus crucial to use the cleaned libraries for any high-precision measurement.

4.3.1. Prior on stellar temperature and metallicity

We test the effects of restricting the templates based on stellar age and metallicity (e.g., age between 1 and 12 Gyrs, and metallicity above 0.1 solar), in order to avoid potential non-physical templates. We have performed this test on SSP libraries as the age of the stars in stellar libraries is not available from the catalogs in the literature. The results of the tests shown in Figure 9 demonstrate that in some cases, non-physical templates (e.g., templates with ages of 15 Gyrs for the XSL SSP library) can be chosen while using the ‘full’ libraries. However, the effect on the inferred stellar velocity dispersion is minimal, well below our target of 1%, with very few exceptions for the XSL models. We thus conclude that it is not necessary to impose a priori cuts on age and metallicity, even though one should be careful in interpreting the results.

⁷ We note that there are some spectra in the full libraries which contain only 0 and NaN. Those need to be excluded to prevent pPXF from crashing.

4.4. Templates

4.4.1. Stellar libraries

The dominant source of potential systematic errors is the choice of templates. Figures 10 to 14 show heat maps representing the average difference in stellar velocity dispersion between any pair of combination of stellar templates. For the MUSE, KCWI, and SDSS samples, the difference averaged over the galaxy sample is reported, while for JWST-NIRSpec, the average difference over 21 spaxels is reported.

It is clear that, it is possible to achieve sub-percent agreement among the measurements from the clean stellar libraries, irrespective of the galaxy sample or instrument being considered. The full stellar libraries can be significantly off, highlighting the importance of using clean libraries. This is particularly striking in the case of JWST-NIRSpec, where the differences between clean and full stellar libraries can be ~10–15%.

4.4.2. Single stellar populations models

As shown in Figures 10 to 14, the stellar velocity dispersions based on the SSP models can differ by a few percent from those inferred based on stellar libraries. The difference is more pronounced for the KCWI and SDSS samples than for the MUSE sample. While for the former the SSP libraries give consistently higher stellar velocity dispersions by 2–4%, the differences are smaller for the MUSE sample. In order to investigate the origin of this discrepancy, we considered a subset of the MUSE sample matched in redshift and stellar velocity dispersion to the KCWI sample. For example, if we restrict the MUSE sample to $z < 0.35$ and $220 \text{ km s}^{-1} < \sigma < 310 \text{ km s}^{-1}$, then the stellar vs. SSP ratios get higher and closer to what we found for KCWI: Indo-US vs EMILES SSP: from $-1.7 \pm 0.3\%$ (MUSE-full) to $-2.9 \pm 0.8\%$ (MUSE-restricted), similar to $-3.4 \pm 0.4\%$ obtained for KCWI. The corresponding numbers for MILES vs. EMILES-SSP are: $-2.9 \pm 0.3\%$, $-3.6 \pm 0.8\%$, and $-2.8 \pm 0.5\%$. For XSL vs. EMILES SSP they are: $-2.4 \pm 0.3\%$, $-3.9 \pm 0.8\%$, and $-4.4 \pm 0.4\%$. In all cases, it seems that the SSP “bias” is larger when selecting the higher σ galaxies at lower redshifts. In general, those will have older ages and higher metallicities than their higher- z and lower- σ counterparts, suggesting deficiencies of the SSP libraries in this part of the parameter space. Our sample size is too small to carry out a detailed investigation of the bias between stellar and SSP libraries as a function of galaxy parameters. Hopefully, future studies will address this.

For the time being, we recommend avoiding the SSP models for high precision/accuracy measurements for a number of reasons. First, the SSPs are based on the assumption that spectra are single stellar populations, which is not true in general. Even a linear combination of a few of them may not have sufficient flexibility to describe the star formation history of the galaxy to the level we require. Indeed, as shown above, the SSPs lead to unphysical solutions in some cases, which raises a red flag. Second, the smaller number of SSP templates compared to stellar templates gives less flexibility to reproduce the diversity in metallicity and elemental abundance. Third, the SSPs are a combination of theoretical and empirical spectra, and we think it is more prudent to stick with empirical spectra for high-precision measurements, given the uncertainties in theoretical atmospheres.

In conclusion, SSPs are fine if one is interested in uncertainties at the 2–3% level, but we find that they are not appropriate for sub-percent accuracy.



Fig. 8. Ratio of velocity dispersion measurements between ‘full’ and ‘clean’ XSL (red), MILES (blue), and Indo-US (green) libraries. The markers denote the ratio of the velocity dispersion measurements for individual galaxies in the MUSE sample, and the horizontal dashed lines mark the sample average for each library. While the effect of cleaning the libraries is most prominent for XSL, it is evident that this is a crucial process to achieve high accuracy.

4.5. Wavelength range

The wavelength range used for the fit is often dictated by practical considerations such as instrumental setup, wavelength coverage of the templates, and the need to avoid features from contaminants (3.3). Within these constraints, it is best to choose a wavelength region that contains deep absorption features such as CaHK, the G-band, and the Ca II Triplet. As we discussed above, the choice of polynomial orders to describe multiplicative and additive continuum terms depends on the wavelength region chosen (see Section 4.2). Fortunately, our extensive tests show that once appropriate polynomial orders are selected and clean stellar libraries are employed, the specific choice of the spectral region is a subdominant contribution to the systematic error budget. Small changes in wavelength coverage (i.e., shifts by 100 Å or so) are absolutely negligible for the quality of the data presented here. Even larger changes make a subdominant contribution to the error budget (see also D’Ago et al. 2023, for a similar result).

We can take advantage of the SDSS spectra available from the SDSS database for the 14 galaxies with KCWI spectra to verify the effects of changing significantly the wavelength range. The wavelength ranges adopted vary substantially (3600–4500 Å for KCWI and 3600–5350 Å for SDSS), with the SDSS including important redder features such as the MgB triplet and Fe5270. We cannot go redder with SDSS because the XSL library is not sufficiently well behaved across the dichroic for our target level of precision and accuracy.

In order to ensure a fair comparison, following Knabel et al. (2024), we convolve the KCWI data with a kernel to match the SDSS seeing and then measure the stellar velocity dispersion within a circular aperture of diameter 3″. The SDSS error dominates the uncertainty, since the SDSS SNR is substantially lower than KCWI. For the Indo-US and XSL clean libraries, the stellar

velocity dispersions agree within one σ , while for MILES, the discrepancy is 2.5σ . Given the uncertainties, we see no significant evidence for a difference, although the uncertainty is relatively large. This comparison should be taken with caution and should be repeated with better-quality data, ideally with a larger sample. Knabel et al. (2024) discusses this comparison in more detail. The main conclusion is that the SDSS data for these specific galaxies are not of sufficient quality to measure stellar velocity dispersions with precision and accuracy better than 5%, confirming the initial assessment by (Bolton et al. 2008).

Shajib et al. (2025, in prep) will present a comparison between kinematics obtained with JWST in the Ca II Triplet region and with KCWI in the blue part of the spectrum. Knabel et al. (2024) presents more comparisons between SDSS and KCWI.

In our analysis, we will not discuss the wavelength region much further, although in our suggested recipe, we include a reminder to check for the effects of the wavelength range.

In summary, we consider the following rest-frame spectral ranges. For MUSE and KCWI, we adopt the range 3600–4500 Å, where the quality of the template libraries sets the blue cutoff, and the red cutoff is imposed by the redshift of the targets and the instrumental setup. For JWST, we use the range 8303–8838 Å for reasons discussed in Section 3.3. For SDSS, we consider 3600–5350 Å, taking advantage of the redder coverage to increase the information content of the spectra and avoiding complications from the UVB-VIS dichroic in the XSL templates.

5. A recipe for accurate stellar velocity dispersions

This section describes a recipe to quantify and minimize residual systematic errors and covariance. The recipe consists of a number of steps that will be summarized at the end of the section. At the core of the recipe is a well-established statistical method to marginalize over systematic uncertainties based on informa-

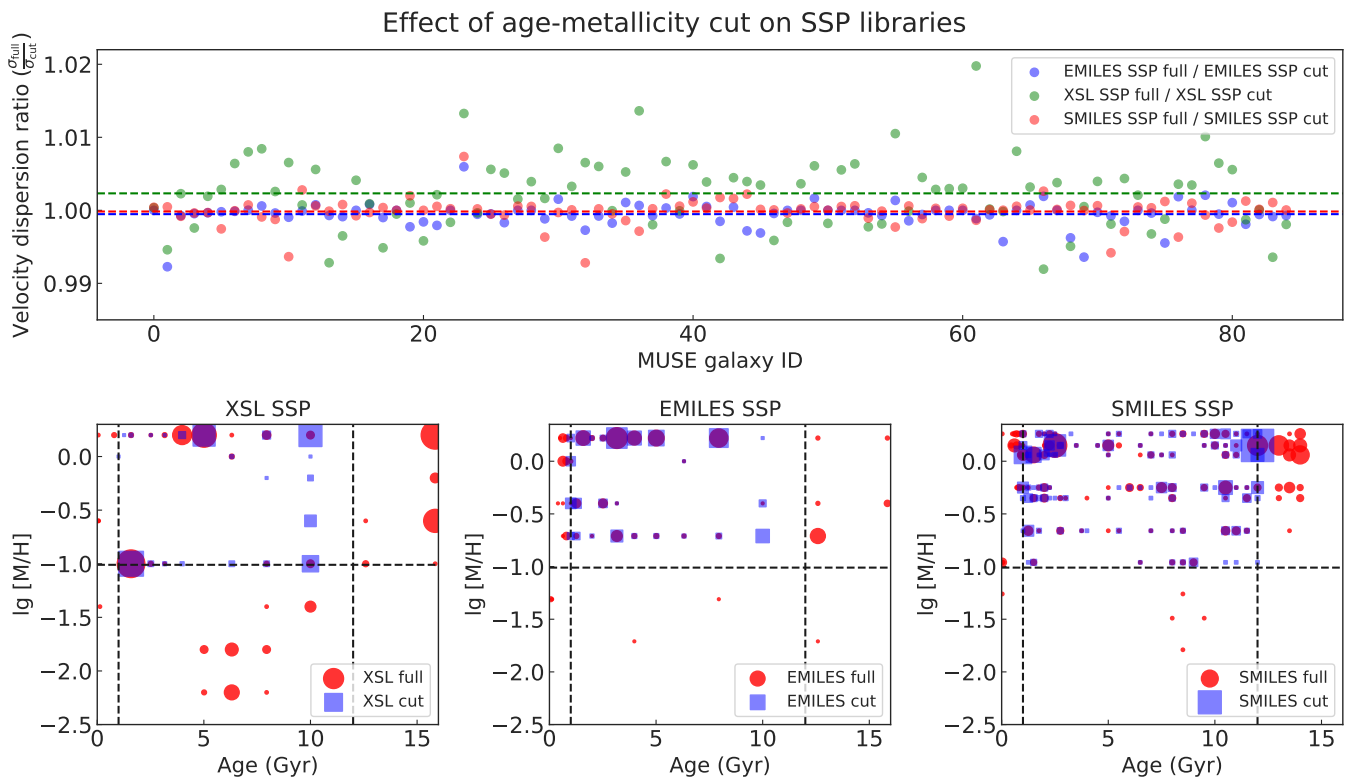


Fig. 9. Comparison of velocity dispersion measurements of the MUSE sample using full E-MILES, sMILES, and XSL SSP libraries vs. the same libraries after applying cuts on age and metallicity of the templates. The top panel shows the ratio of velocity dispersion measurements using the ‘full’ and ‘cut’ SSP libraries. The blue (E-MILES), green (XSL), and red (sMILES) markers show the ratio for individual galaxies, and the dashed lines represent the sample average for each library. In almost all cases, the effect of the cut is sub-percent. The three panels at the bottom show the age and metallicity of the templates selected by pPXF to fit our spectra, and they correspond to XSL, E-MILES, and sMILES SSP libraries from left to right. The red circles and green squares are for ‘full’ and ‘cut’ libraries, respectively, where the size of the marker in each panel is proportional to how many times the corresponding template was used. The black dashed lines show the age and metallicity restriction applied to the ‘cut’ libraries. For E-MILES and sMILES, in general, the same templates were selected with similar frequency regardless of which version of the corresponding library was used. As a result, the ratios for individual galaxies (blue and red circles on the top panel) are very close to 1 for almost all galaxies. For XSL, the difference in velocity dispersions from ‘full’ and ‘cut’ libraries are somewhat higher compared to the other two libraries, but still well below our target of 1%.

tion contained in the data themselves. The reader not interested in the statistical details can skip directly to the final end product described in Section 6 and in Table 2, where we summarize the results obtained with our method, and those that one would obtain by the simplest approach – a straight average of the fits obtained with the three clean stellar libraries.

In practice, we consider the possible choice of template as a nuisance parameter and marginalize over it weighted by the probability of the model given the data. However, since the data and model parameters vary, to obtain a fair marginalization we cannot use a simple likelihood ratio, but we need to use a more general metric. Following, e.g., [Birrer et al. \(2019\)](#), we assign the statistical weight w based on the Bayesian information criterion (BIC), defined as ([Schwarz 1978](#)):

$$\text{BIC} = k \ln(n) - 2 \ln(\hat{L}), \quad (4)$$

where k is the number of free parameters in the model, n represents the number of data points (or pixels), and \hat{L} stands for the maximum value of the likelihood function, corresponding to the model.

Note that for a sample of galaxies, one has to construct the BIC for the whole sample since the first term of the right-hand

side of [Equation 4](#) is non-linear in n . In other words, if there are N galaxies in the sample with n_i data points each, and they are each fit with k_i degrees of freedom resulting in likelihood \hat{L}_i the equation becomes:

$$\text{BIC} = \left(\sum_i k_i \right) \ln \left(\sum_i n_i \right) - 2 \sum_i \ln \hat{L}_i. \quad (5)$$

The likelihood term is effectively a χ^2 with an important caveat. Standard practice in kinematics fits is to scale the noise levels by a multiplicative factor so that the χ^2 per degree of freedom is one, in order to account for potential error under/overestimates. We adopt this practice, but we are careful to adopt the same multiplicative factor for a given galaxy across all our tests, to retain the information provided by the difference in χ^2 across fits.

5.1. Counting free parameters

The definition of the number of free parameters in the BIC is non-trivial and requires some discussion. The parameter n is the number of spectral points used in the fit, after masking. The number of free model parameters k is given by $k = M + N_{\text{poly}} + N_{\text{temp}}$, where the M is typically 2 and accounts for the stellar veloc-

MUSE velocity dispersion (row-column)/column

	Indo-US clean	MILES clean	XSL clean	Indo-US full	MILES full	XSL full	SMILES	EMILES SSP cut	XSL SSP cut	SMILES SSP cut	EMILES SSP full	XSL SSP full	SMILES SSP full
Indo-US clean	-	1.2% (±0.3)	0.7% (±0.3)	-0.0% (±0.3)	1.6% (±0.3)	-1.3% (±0.3)	1.3% (±0.3)	-1.7% (±0.3)	0.8% (±0.3)	-0.6% (±0.3)	-1.7% (±0.3)	0.6% (±0.3)	-0.6% (±0.3)
MILES clean	-1.2% (±0.3)	-	-0.5% (±0.3)	-1.2% (±0.3)	0.4% (±0.3)	-2.4% (±0.3)	0.2% (±0.3)	-2.9% (±0.3)	-0.3% (±0.3)	-1.8% (±0.3)	-2.8% (±0.3)	-0.6% (±0.3)	-1.8% (±0.3)
XSL clean	-0.6% (±0.3)	0.5% (±0.3)	-	-0.7% (±0.3)	0.9% (±0.3)	-1.9% (±0.3)	0.7% (±0.3)	-2.3% (±0.3)	0.2% (±0.3)	-1.3% (±0.3)	-2.3% (±0.3)	-0.0% (±0.3)	-1.2% (±0.3)
Indo-US full	0.1% (±0.3)	1.2% (±0.3)	0.7% (±0.3)	-	1.6% (±0.3)	-1.2% (±0.3)	1.4% (±0.3)	-1.7% (±0.3)	0.9% (±0.3)	-0.6% (±0.3)	-1.6% (±0.3)	0.7% (±0.3)	-0.6% (±0.3)
MILES full	-1.5% (±0.3)	-0.4% (±0.3)	-0.9% (±0.3)	-1.6% (±0.3)	-	-2.8% (±0.3)	-0.2% (±0.3)	-3.2% (±0.3)	-0.7% (±0.3)	-2.1% (±0.3)	-3.2% (±0.3)	-0.9% (±0.3)	-2.1% (±0.3)
XSL full	1.4% (±0.3)	2.6% (±0.3)	2.0% (±0.3)	1.3% (±0.3)	2.9% (±0.3)	-	2.7% (±0.3)	-0.4% (±0.3)	2.2% (±0.3)	0.7% (±0.3)	-0.3% (±0.3)	2.0% (±0.3)	0.8% (±0.3)
SMILES	-1.3% (±0.3)	-0.1% (±0.3)	-0.7% (±0.3)	-1.4% (±0.3)	0.2% (±0.3)	-2.6% (±0.3)	-	-3.0% (±0.3)	-0.5% (±0.3)	-1.9% (±0.3)	-3.0% (±0.3)	-0.7% (±0.3)	-1.9% (±0.3)
EMILES SSP cut	1.8% (±0.3)	3.0% (±0.3)	2.4% (±0.3)	1.7% (±0.3)	3.4% (±0.3)	0.5% (±0.3)	3.1% (±0.3)	-	2.6% (±0.3)	1.1% (±0.3)	0.1% (±0.3)	2.4% (±0.3)	1.1% (±0.3)
XSL SSP cut	-0.8% (±0.3)	0.4% (±0.3)	-0.2% (±0.3)	-0.9% (±0.3)	0.7% (±0.3)	-2.1% (±0.3)	0.5% (±0.3)	-2.5% (±0.3)	-	-1.4% (±0.3)	-2.5% (±0.3)	-0.2% (±0.3)	-1.4% (±0.3)
SMILES SSP cut	0.7% (±0.3)	1.8% (±0.3)	1.3% (±0.3)	0.6% (±0.3)	2.2% (±0.3)	-0.6% (±0.3)	2.0% (±0.3)	-1.1% (±0.3)	1.5% (±0.3)	-	-1.0% (±0.3)	1.3% (±0.3)	0.0% (±0.3)
EMILES SSP full	1.7% (±0.3)	2.9% (±0.3)	2.4% (±0.3)	1.7% (±0.3)	3.3% (±0.3)	0.4% (±0.3)	3.1% (±0.3)	-0.1% (±0.3)	2.6% (±0.3)	1.1% (±0.3)	-	2.3% (±0.3)	1.1% (±0.3)
XSL SSP full	-0.6% (±0.3)	0.6% (±0.3)	0.1% (±0.3)	-0.6% (±0.3)	1.0% (±0.3)	-1.9% (±0.3)	0.7% (±0.3)	-2.3% (±0.3)	0.2% (±0.3)	-1.2% (±0.3)	-2.3% (±0.3)	-	-1.2% (±0.3)
SMILES SSP full	0.7% (±0.3)	1.8% (±0.3)	1.3% (±0.3)	0.6% (±0.3)	2.2% (±0.3)	-0.7% (±0.3)	2.0% (±0.3)	-1.1% (±0.3)	1.5% (±0.3)	-0.0% (±0.3)	-1.1% (±0.3)	1.2% (±0.3)	-

Fig. 10. Comparison of velocity dispersion measurements of the MUSE sample using a range of template libraries. For every pair of libraries, the heat map shows the relative difference in the inferred stellar velocity dispersion, averaged across the sample. The uncertainty is estimated by bootstrap resampling the galaxies. Blue (red) boxes represent pairs in which the library listed on the row yields a lower (higher) value than that listed on the column. The wavelength range is 3600–4500 Å.

ity dispersion and line-of-sight velocity (but it could be more if there are multiple components, see, e.g., Shajib et al. 2025), N_{poly} is the number of corrective polynomial orders (both additive and multiplicative), and N_{temp} is the number of “significant templates,” i.e., the number of nonzero templates, or in practice the number of templates that contribute above a certain threshold (in our case 1%) to the fit. The threshold is needed for two reasons. First, stellar libraries can include a large number of spectra

that are not relevant to fit the data (e.g., B stars), and those should not be counted in order to obtain a fair representation of the effective freedom of the fit.

Second, from a numerical standpoint, the rationale for omitting the weights of zero or nearly-zero templates when estimating free parameters is that when a template weight reaches the boundary at the optimal fit, the positivity constraint in the template fit behaves like an equality constraint. This effectively elim-

KCWI velocity dispersion (row-column)/column

	Indo-US clean	MILES clean	XSL clean	Indo-US full	MILES full	XSL full	sMILES	E-MILES SSP cut	XSL SSP cut	sMILES SSP cut	E-MILES SSP full	XSL SSP full	sMILES SSP full
Indo-US clean	-	-0.7% (± 0.3)	1.1% (± 0.2)	-0.3% (± 0.2)	-0.1% (± 0.3)	0.4% (± 0.3)	0.4% (± 0.3)	-3.4% (± 0.5)	0.1% (± 0.5)	-2.1% (± 0.6)	-3.4% (± 0.5)	-0.4% (± 0.5)	-2.1% (± 0.6)
MILES clean	0.7% (± 0.3)	-	1.7% (± 0.2)	0.4% (± 0.3)	0.6% (± 0.3)	1.1% (± 0.4)	1.1% (± 0.3)	-2.8% (± 0.5)	0.7% (± 0.5)	-1.5% (± 0.6)	-2.7% (± 0.5)	0.3% (± 0.5)	-1.5% (± 0.6)
XSL clean	-1.0% (± 0.2)	-1.7% (± 0.2)	-	-1.3% (± 0.2)	-1.1% (± 0.2)	-0.6% (± 0.3)	-0.7% (± 0.2)	-4.4% (± 0.5)	-1.0% (± 0.5)	-3.1% (± 0.6)	-4.4% (± 0.5)	-1.4% (± 0.5)	-3.1% (± 0.6)
Indo-US full	0.3% (± 0.2)	-0.4% (± 0.3)	1.3% (± 0.2)	-	0.2% (± 0.3)	0.7% (± 0.3)	0.7% (± 0.3)	-3.2% (± 0.5)	0.3% (± 0.5)	-1.8% (± 0.6)	-3.1% (± 0.5)	-0.1% (± 0.5)	-1.8% (± 0.6)
MILES full	0.1% (± 0.3)	-0.6% (± 0.3)	1.1% (± 0.2)	-0.2% (± 0.3)	-	0.5% (± 0.4)	0.5% (± 0.3)	-3.4% (± 0.5)	0.1% (± 0.6)	-2.0% (± 0.6)	-3.3% (± 0.6)	-0.3% (± 0.6)	-2.0% (± 0.6)
XSL full	-0.4% (± 0.3)	-1.1% (± 0.4)	0.6% (± 0.3)	-0.7% (± 0.3)	-0.5% (± 0.4)	-	-0.0% (± 0.4)	-3.9% (± 0.5)	-0.4% (± 0.6)	-2.5% (± 0.6)	-3.8% (± 0.6)	-0.8% (± 0.6)	-2.5% (± 0.6)
sMILES	-0.4% (± 0.3)	-1.0% (± 0.3)	0.7% (± 0.2)	-0.7% (± 0.3)	-0.5% (± 0.3)	0.0% (± 0.4)	-	-3.8% (± 0.5)	-0.3% (± 0.5)	-2.5% (± 0.6)	-3.8% (± 0.5)	-0.7% (± 0.5)	-2.5% (± 0.6)
E-MILES SSP cut	3.6% (± 0.5)	2.9% (± 0.5)	4.6% (± 0.5)	3.3% (± 0.5)	3.5% (± 0.6)	4.0% (± 0.6)	4.0% (± 0.6)	-	3.6% (± 0.7)	1.4% (± 0.8)	0.0% (± 0.7)	3.2% (± 0.7)	1.4% (± 0.8)
XSL SSP cut	-0.1% (± 0.5)	-0.7% (± 0.5)	1.0% (± 0.5)	-0.3% (± 0.5)	-0.1% (± 0.6)	0.4% (± 0.6)	0.3% (± 0.5)	-3.5% (± 0.7)	-	-2.2% (± 0.7)	-3.5% (± 0.7)	-0.4% (± 0.7)	-2.2% (± 0.7)
sMILES SSP cut	2.2% (± 0.6)	1.5% (± 0.6)	3.2% (± 0.6)	1.9% (± 0.6)	2.1% (± 0.6)	2.6% (± 0.7)	2.6% (± 0.6)	-1.3% (± 0.7)	2.2% (± 0.8)	-	-1.3% (± 0.8)	1.8% (± 0.8)	0.0% (± 0.8)
E-MILES SSP full	3.5% (± 0.6)	2.8% (± 0.6)	4.6% (± 0.5)	3.2% (± 0.6)	3.4% (± 0.6)	4.0% (± 0.6)	3.9% (± 0.6)	-0.0% (± 0.7)	3.6% (± 0.7)	1.3% (± 0.8)	-	3.1% (± 0.7)	1.3% (± 0.8)
XSL SSP full	0.4% (± 0.5)	-0.3% (± 0.5)	1.4% (± 0.5)	0.1% (± 0.5)	0.3% (± 0.6)	0.8% (± 0.6)	0.7% (± 0.6)	-3.1% (± 0.7)	0.4% (± 0.7)	-1.8% (± 0.8)	-3.0% (± 0.7)	-	-1.8% (± 0.8)
sMILES SSP full	2.2% (± 0.6)	1.5% (± 0.6)	3.2% (± 0.6)	1.9% (± 0.6)	2.1% (± 0.6)	2.6% (± 0.7)	2.6% (± 0.6)	-1.3% (± 0.7)	2.2% (± 0.8)	0.0% (± 0.8)	-1.3% (± 0.8)	1.8% (± 0.8)	-

Fig. 11. Comparison of velocity dispersion measurements of the KCWI sample using a range of template libraries. The wavelength range is 3600–4500 Å. This figure is in the same format as Figure 10.

inates one free parameter. During the constrained quadratic template optimization, pPXF identifies the optimal weights by aiming to minimize the χ^2 to machine precision. This process can result in some very small weights, which, while formally necessary to optimize χ^2 , make no significant contribution to the fit from a physical perspective.

Intuitively, the threshold is related to the noise level of the galaxy spectra. For our data quality SNR 30–160 Å⁻¹ (i.e., 1–3% per Å), we find that 1% is the appropriate threshold using the following procedure. We first carry out a pPXF fit with all

the templates in the library, and then we repeat the fit by keeping the spectra that contribute only above a certain threshold to the initial fit. As expected, we find that for a high threshold (10–20%), the BIC is large because there are not enough templates to obtain a good fit. Conversely, below $\sim 1\%$, the χ^2 does not improve enough to compensate for the increased number of degrees of freedom in the BIC. This threshold depends on the quality of the data, approximately in a manner inversely proportional to the SNR. We recommend following our procedure to set the threshold for each specific dataset.

SDSS velocity dispersion (row-column)/column

	Indo-US clean	MILES clean	XSL clean	Indo-US full	MILES full	XSL full	sMILES	E-MILES SSP cut	XSL SSP cut	sMILES SSP cut	E-MILES SSP full	XSL SSP full	sMILES SSP full
Indo-US clean	-	-1.9% (± 0.2)	1.2% (± 0.2)	0.2% (± 0.3)	-0.7% (± 0.3)	1.0% (± 0.3)	-1.2% (± 0.3)	-6.3% (± 0.3)	-3.3% (± 0.3)	-5.0% (± 0.3)	-6.2% (± 0.3)	-3.2% (± 0.3)	-5.0% (± 0.3)
MILES clean	2.0% (± 0.2)	-	3.2% (± 0.3)	2.2% (± 0.4)	1.2% (± 0.4)	3.0% (± 0.3)	0.7% (± 0.3)	-4.4% (± 0.3)	-1.4% (± 0.4)	-3.1% (± 0.4)	-4.4% (± 0.3)	-1.3% (± 0.3)	-3.1% (± 0.4)
XSL clean	-1.2% (± 0.2)	-3.1% (± 0.3)	-	-1.0% (± 0.3)	-1.9% (± 0.3)	-0.2% (± 0.3)	-2.4% (± 0.3)	-7.4% (± 0.3)	-4.5% (± 0.3)	-6.1% (± 0.3)	-7.4% (± 0.3)	-4.4% (± 0.3)	-6.1% (± 0.3)
Indo-US full	-0.2% (± 0.3)	-2.2% (± 0.3)	1.0% (± 0.4)	-	-1.0% (± 0.4)	0.8% (± 0.4)	-1.5% (± 0.4)	-6.5% (± 0.4)	-3.6% (± 0.4)	-5.2% (± 0.4)	-6.5% (± 0.4)	-3.5% (± 0.4)	-5.2% (± 0.4)
MILES full	0.8% (± 0.3)	-1.2% (± 0.3)	2.0% (± 0.3)	1.0% (± 0.4)	-	1.8% (± 0.4)	-0.5% (± 0.4)	-5.6% (± 0.4)	-2.6% (± 0.4)	-4.3% (± 0.4)	-5.5% (± 0.4)	-2.5% (± 0.4)	-4.3% (± 0.4)
XSL full	-1.0% (± 0.3)	-2.9% (± 0.3)	0.2% (± 0.3)	-0.8% (± 0.4)	-1.7% (± 0.4)	-	-2.2% (± 0.4)	-7.2% (± 0.4)	-4.3% (± 0.4)	-5.9% (± 0.4)	-7.2% (± 0.3)	-4.2% (± 0.4)	-5.9% (± 0.4)
sMILES	1.3% (± 0.3)	-0.7% (± 0.3)	2.5% (± 0.3)	1.5% (± 0.4)	0.5% (± 0.4)	2.3% (± 0.4)	-	-5.1% (± 0.4)	-2.1% (± 0.4)	-3.8% (± 0.4)	-5.1% (± 0.4)	-2.0% (± 0.4)	-3.8% (± 0.4)
E-MILES SSP cut	6.7% (± 0.3)	4.7% (± 0.4)	8.0% (± 0.4)	7.0% (± 0.4)	5.9% (± 0.4)	7.8% (± 0.4)	5.4% (± 0.4)	-	3.1% (± 0.4)	1.4% (± 0.4)	0.1% (± 0.4)	3.2% (± 0.4)	1.4% (± 0.4)
XSL SSP cut	3.5% (± 0.3)	1.5% (± 0.4)	4.7% (± 0.4)	3.7% (± 0.4)	2.7% (± 0.4)	4.5% (± 0.4)	2.2% (± 0.4)	-3.0% (± 0.4)	-	-1.7% (± 0.4)	-3.0% (± 0.4)	0.1% (± 0.4)	-1.7% (± 0.4)
sMILES SSP cut	5.2% (± 0.3)	3.2% (± 0.4)	6.5% (± 0.4)	5.5% (± 0.4)	4.5% (± 0.4)	6.3% (± 0.4)	3.9% (± 0.4)	-1.4% (± 0.4)	1.7% (± 0.4)	-	-1.3% (± 0.4)	1.8% (± 0.4)	0.0% (± 0.4)
E-MILES SSP full	6.6% (± 0.3)	4.6% (± 0.4)	8.0% (± 0.4)	6.9% (± 0.4)	5.8% (± 0.4)	7.7% (± 0.4)	5.3% (± 0.4)	-0.1% (± 0.4)	3.1% (± 0.4)	1.3% (± 0.4)	-	3.2% (± 0.4)	1.3% (± 0.4)
XSL SSP full	3.4% (± 0.3)	1.4% (± 0.3)	4.6% (± 0.4)	3.6% (± 0.4)	2.6% (± 0.4)	4.4% (± 0.4)	2.1% (± 0.4)	-3.1% (± 0.4)	-0.1% (± 0.4)	-1.8% (± 0.4)	-3.1% (± 0.4)	-	-1.8% (± 0.4)
sMILES SSP full	5.2% (± 0.3)	3.2% (± 0.4)	6.5% (± 0.4)	5.5% (± 0.4)	4.5% (± 0.4)	6.3% (± 0.4)	3.9% (± 0.4)	-1.4% (± 0.4)	1.7% (± 0.4)	0.0% (± 0.4)	-1.3% (± 0.4)	1.8% (± 0.4)	-

Fig. 12. Comparison of velocity dispersion measurements of the sample with SDSS spectra with $S/N > 15 \text{ \AA}^{-1}$, using a range of template libraries. The wavelength range is 3600-5350 Å. Same format as Figure 10.

5.2. Computing the weights

The probability of a model F_i given the data is formulated as:

$$P(F_i|\mathbf{d}) \propto P(\mathbf{d}|F_i)P(F_i) \approx \exp\left[-\frac{1}{2}\text{BIC}_i\right]P(F_i). \quad (6)$$

Hence, the relative probability between two fits, F_1 and F_2 , given the data, can be written in terms of the fits' corresponding BIC values:

$$\frac{P(F_1|\mathbf{d})}{P(F_2|\mathbf{d})} = \exp\left[-\frac{1}{2}(\text{BIC}_1 - \text{BIC}_2)\right]. \quad (7)$$

However, we only have a noisy estimate of the BIC, with the noise given by statistical noise and sampling noise. Thus, we need to define the evidence ratio function $f(x)$ in terms of a

JWST NIRSpec velocity dispersion (row-column)/column

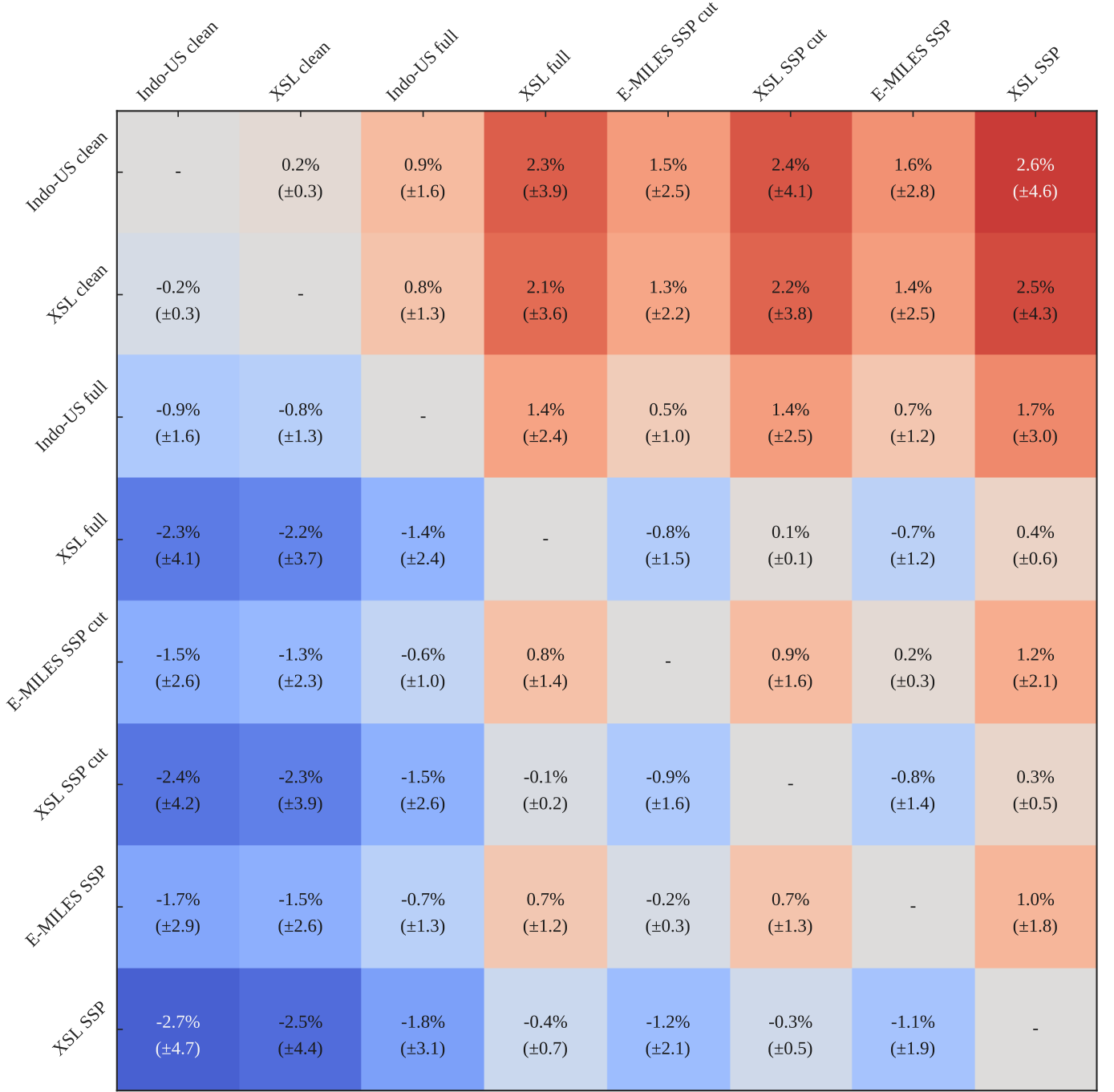


Fig. 13. Comparison of velocity dispersion measurements for the JWST/NIRSpec spectra for RXJ1131–1231. The differences in the measured dispersions are averaged over 21 spaxels within a $0''.5 \times 0''.5$ square at the center of the lens galaxy. This figure is in the same format as Figure 10, except that fewer libraries are shown, only the ones that include the wavelength region of the Ca II triplet used to fit the JWST/NIRSpec data.

variable x sampling the “true” difference between a fit’s corresponding BIC value and the lowest BIC among all possible fit configurations as discussed above, $\text{BIC}_{\min,k}$:

$$f(x) \equiv \begin{cases} 1 & , x \leq 0, \\ \exp\left[-\frac{1}{2}(x)\right] & , x > 0. \end{cases} \quad (8)$$

To find a model’s associated statistical weight, w_k , we marginalize over x , with the probability of x given the measured

ΔBIC_k described by a Gaussian, g , centered on ΔBIC_k with a variance of $\sigma_{\Delta\text{BIC},k}^2$.

The standard deviation, $\sigma_{\Delta\text{BIC},k}$, represents the uncertainty in the ΔBIC calculation and is dominated by numerical effects and population sampling. There could be, for example, one galaxy with unusual abundance ratios that is the best fit by a lucky template and skews the BIC. In contrast to the strong lensing cases described by Birrer et al. (2019) and Shajib et al. (2022), convergence is not an issue for the kinematic fits described here. The

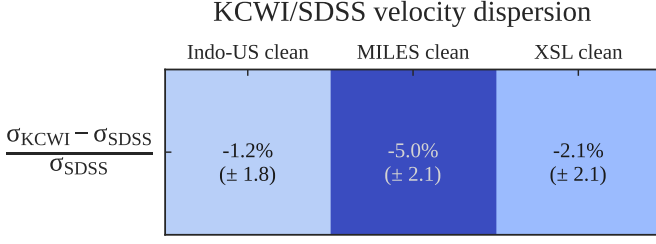


Fig. 14. Comparison of the velocity dispersion measured from the KCWI and SDSS spectra of the same galaxies, using the three “clean” stellar libraries. Note that SDSS and KCWI cover two different wavelength ranges (3600–5350 Å and 3600–4500 Å, respectively). The KCWI data have been convolved to match the SDSS seeing and integrated within the SDSS fiber for a fair comparison. Though the difference in the case of MILES is relatively large, we stress that SDSS data for these specific galaxies are not of sufficient quality to measure stellar velocity dispersions with precision and accuracy better than 5%.

BIC uncertainty can then simply be estimated by bootstrap resampling the sample of galaxies. Importantly, there is covariance between the BIC calculated using a pair of stellar libraries: some galaxies may be better fit by more than one template library than others, and therefore, one needs to compute the scatter in ΔBIC by bootstrap resampling the sample of galaxies, rather than computing the scatter independently for each library. Typically, we find $\sigma_{\Delta\text{BIC}} = 100\text{--}200$ for the samples under consideration here, although clearly, the BIC and its uncertainty depend on sample size.

The marginalization over x is given by the integral:

$$w_k = \int f(x) \frac{1}{\sqrt{2\pi}\sigma_{\Delta\text{BIC},k}} \exp\left[-\frac{1}{2}\left(\frac{x - \Delta\text{BIC}_k}{\sigma_{\Delta\text{BIC},k}}\right)^2\right] dx. \quad (9)$$

The integral can be simplified analytically to gather some insight and for numerical precision. We set for simplicity of notation $\Delta := \Delta\text{BIC}_k$ and $\sigma := \sigma_{\Delta\text{BIC},k}$. The part for $x \leq 0$ is simply the integral of a Gaussian, simplified by setting $y = (x - \Delta)/\sigma$, while the part for $x > 0$ can be solved by setting $z = (x - \Delta)/\sigma + \sigma/2$ to obtain

$$w_k = \int_{-\infty}^{-\Delta/\sigma} \frac{e^{-y^2/2}}{\sqrt{2\pi}} dy + \exp\left[\frac{\sigma^2}{8} - \frac{\Delta}{2}\right] \int_{-\Delta/\sigma + \sigma/2}^{\infty} \frac{e^{-z^2/2}}{\sqrt{2\pi}} dz. \quad (10)$$

If Δ is much larger than σ (i.e., if a BIC is significantly worse than the best BIC), then the first term becomes negligible, and the second term behaves as an exponential down-weight.

Having defined the weights, the mean $\bar{\sigma}$, systematic uncertainty $\Delta\bar{\sigma}$, and statistical uncertainty $\delta\bar{\sigma}$ of the velocity dispersion of an individual galaxy is given by the standard expressions

$$\bar{\sigma} = \frac{\sum_k w_k \sigma_k}{\sum_k w_k} \quad (11)$$

$$(\Delta\bar{\sigma})^2 = \frac{\sum_k w_k (\sigma_k - \bar{\sigma})^2}{\sum_k w_k}, \quad (12)$$

and

$$\delta\bar{\sigma} = \sqrt{\frac{\sum_k w_k (\delta\sigma_k)^2}{\sum_k w_k}}, \quad (13)$$

where the index k runs through the choices (e.g., template library), and $\delta\sigma_k$ is the statistical uncertainty estimated by pPXF. For an individual system, the total error is given by the quadratic sum of the systematic and statistical errors.

When the number of template libraries is small (as in the case considered here), it is prudent to adopt Bessel’s correction to get the unbiased estimators (see Appendix A for a derivation)

$$(\Delta_B \bar{\sigma})^2 = \frac{\sum_k w_k (\sigma_k - \bar{\sigma})^2}{\sum_k w_k - \sum_k w_k^2 / \sum_k w_k}. \quad (14)$$

For a sample of galaxies or multiple spatial bins within a galaxy, in addition to measuring the average the mean $\bar{\sigma}_i$, one can estimate the the covariance matrix as:

$$C_{ij} \bar{\sigma} = \frac{\sum_k w_k (\sigma_{k,i} - \bar{\sigma}_i)(\sigma_{k,j} - \bar{\sigma}_j)}{\sum_k w_k} + \delta_{i,j} \delta\bar{\sigma}_i^2, \quad (15)$$

where the indexes i, j identify the elements of the covariance matrix, and $\delta_{i,j}$ is the Kronecker’s delta function. Along the diagonal, the first term is the systematic error, and the second is the statistical error.

For a small number of stellar libraries, again, we recommend Bessel’s corrected estimator, which reads

$$C_{B,i,j} \bar{\sigma} = \frac{\sum_k w_k (\sigma_{k,i} - \bar{\sigma}_i)(\sigma_{k,j} - \bar{\sigma}_j)}{\sum_k w_k - \sum_k w_k^2 / \sum_k w_k} + \delta_{i,j} \delta\bar{\sigma}_i^2. \quad (16)$$

5.3. Verifying polynomial orders setting

Our tests show that the BIC does not vary sufficiently to distinguish polynomial orders. This is understandable in terms of mathematical degeneracies: within plausible ranges, all polynomial orders give good fits. However, if the polynomial orders are too low or too high, they will artificially enhance the discrepancy between the results of applying different templates. Therefore, it is important to choose a combination of polynomial orders in the range where the stellar velocity dispersion is stable and the scatter between templates ($\Delta\bar{\sigma}/\bar{\sigma}$) is smallest.

For a sample of galaxies or multiple spatial bins within a galaxy, identified by the subscript i , one would have to compute the average σ_k across the sample $\langle \sigma_k \rangle_i$, then compute the weighted average of it across templates index k using the global BIC,

$$\langle \bar{\sigma} \rangle_i = \frac{\sum_k w_k \langle \sigma_k \rangle_i}{\sum_k w_k}, \quad (17)$$

and the systematic uncertainty on the mean

$$(\Delta \langle \sigma \rangle_i)^2 = \frac{\sum_k w_k (\langle \sigma_k \rangle_i - \langle \bar{\sigma} \rangle_i)^2}{\sum_k w_k}. \quad (18)$$

For a small number of stellar libraries, as in the case discussed here, we recommend applying Bessel’s correction:

$$(\Delta_B \langle \sigma \rangle_i)^2 = \frac{\sum_k w_k (\langle \sigma_k \rangle_i - \langle \bar{\sigma} \rangle_i)^2}{\sum_k w_k - \sum_k w_k^2 / \sum_k w_k}. \quad (19)$$

In the end, it is important to verify that the combination of polynomial orders $\Delta \langle \sigma \rangle_i / \langle \bar{\sigma} \rangle_i$ is around the minimum

within the uncertainty. In Figures 15 and 16, we show as an example the dependency of the inferred stellar velocity dispersion as a function of polynomial orders for the MUSE sample. The left-hand side panel shows the BIC-weighted average of the three clean stellar libraries, while the right-hand side panel shows the straight average. In all cases, the results change much less than 1% for polynomial orders around our fiducial values. Bessel-corrected estimators have been used.

5.4. Summary of Recipe

Here, we summarize our suggested recipe step-by-step to obtain accurate and precise stellar velocity dispersion –

1. Use data with sufficient signal-to-noise ratio. If the signal-to-noise ratio is too low, the inference will not only be more noisy, but can also be biased. The precise threshold depends on the wavelength coverage and spectral resolution of the dataset and also on the target accuracy and precision. This can be estimated by simulations or checked post-facto using this recipe itself, varying the threshold in SNR.
2. Use clean stellar template libraries. Popular stellar libraries include spectra that may be interesting for other applications, but have insufficient quality for precise and accurate determination. We provide our “clean” list for MILES, XSL, and Indo-Us through GitHub, with the caveat that additional cuts/masking may be required depending on the wavelength and quality of the data under consideration.
3. Run initial tests on additional and multiplicative polynomial orders to identify the range in which the results are stable. Depending on the wavelength range and quality of the data, it may be necessary to marginalize over polynomial orders while computing the total systematic error budget.
4. Measure the stellar velocity dispersion with all the high-quality (clean) stellar libraries that have sufficient resolution and wavelength coverage for the data set.
5. Compute the Bayesian Information Criterion to evaluate the relative goodness of fit of the data for each of the template libraries.
6. Estimate the systematic error associated with template libraries, and correlation between multiple galaxies or spatial bins, using the Equations provided in this Section.
7. (Optional) If the systematic error associated with the template library is smaller than 0.5%, and a better estimate of the systematic error is needed, compute the additional term by evaluating residual scatter by marginalizing over polynomial orders and small changes in the wavelength range.

6. Results

In this section, we summarize and discuss our main results, namely the precision and accuracy of the stellar velocity dispersion measurements obtained by applying our recipe to our datasets. We stress that, whereas the recipe is general and can be applied to any dataset, the precision and accuracy that can be achieved are specific to each dataset, and depend on the signal-to-noise ratio, resolution, wavelength range, and intrinsic properties of the galaxy spectra under consideration. We will, therefore, first discuss each dataset separately and then draw some general conclusions. The key numbers are summarized in Table 2. For convenience, we report both the values obtained with our optimal recipe and also those obtained with a straight average of the three clean stellar libraries.

6.1. MUSE

For the MUSE sample, we find the average statistical uncertainty to be of order 2%. This is not surprising, given the quality of the dataset. We find that the data prefer the Indo-US library over the XSL library and strongly disfavor the MILES library. We note that this preference is made possible by the large dataset. If we had a single galaxy, the difference in BIC would be much less statistically significant.

The BIC-weighted average systematic error is much smaller than our target of 1%, even with Bessel correction. This is, of course, only the error associated with template choice. Other potential sources of error at the level of 0.2-0.5% are the wavelength range, instrumental resolution, and polynomial order, and those should be investigated if one wants to push accuracy to the level of 0.3-0.4%.

Not surprisingly, the velocity dispersion has positive covariance across the sample: templates that yield higher (lower) velocity dispersion do so consistently for all galaxies. Importantly, the amplitude of the covariance is also well below 1%.

If one were to ignore the information from the BIC and weigh the three clean stellar libraries equally, the uncertainties associated with the stellar template would increase to the values indicated in the lower part of Table 2. The increase is noticeable and strengthens the importance of adopting our proposed recipe. However, even with this suboptimal weight, the systematic errors and off-diagonal elements of the covariance matrix remain sub-percent.

6.1.1. KCWI

The results for KCWI are very similar to those obtained for MUSE, with the main difference being that Indo-US is now more strongly favored with respect to both XSL and MILES. This may be due to the superior SNR of the data, reflected in the sub-percent statistical errors. Since the data tell us that they clearly prefer Indo-US, then the residual systematics obtained with our procedure are vanishingly small, and Bessel correction is crucial to obtain a realistic estimate of the systematic error. For comparison, a straight average of the three clean stellar libraries leaves systematic residual uncertainties and covariance below 1%.

6.2. NIRSpec

For the NIRSpec data, we find sub-percent systematic errors and off-diagonal elements, similar to all the other datasets considered in this paper. The average random uncertainty is ~6% per spaxel. Although this level is higher than that of other samples, this is driven by the somewhat lower signal-to-noise ratio of the single spaxels in the NIRSpec data, and by the QSO contamination. The random uncertainty can be decreased by summing over multiple spaxels, albeit at the loss of spatial resolution. BIC-weighting prefers XSL over Indo-US only marginally.

6.3. SDSS

The results for SDSS are qualitatively in line with the other instruments, even though the accuracy and precision is lower, as expected given that the SNR of the data is significantly lower. As expected, average random errors are higher than MUSE and KCWI, between 3-4%. Remarkably, even with the lower data quality, systematic errors and covariance are just above 1% for BIC weighting and still below 2% with the straight average. The most significant difference is that the SDSS spectra prefer

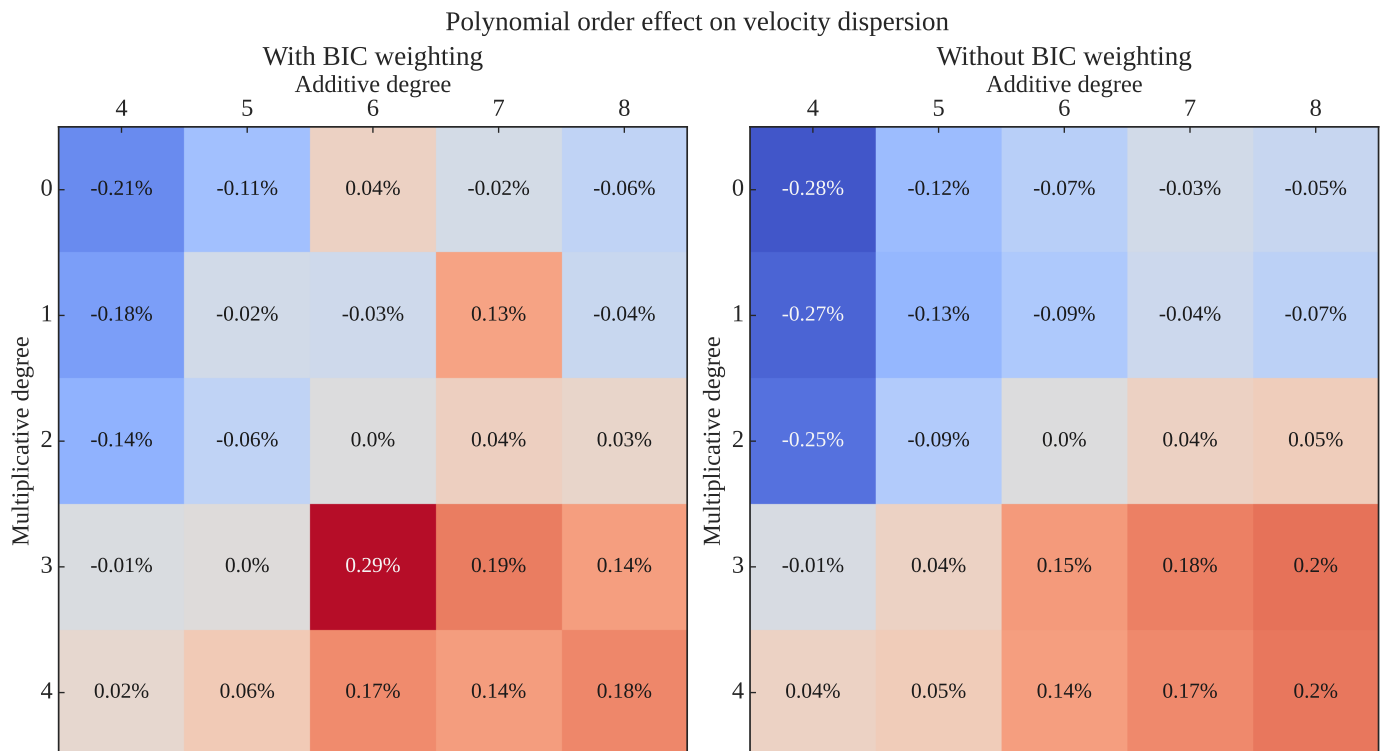


Fig. 15. Dependency of the average stellar velocity dispersion inferred for the MUSE sample as a function of polynomial orders, relative to the fiducial setting. The variations are much smaller than 1%, with and without BIC weighting.

Table 2. Summary of results. For each dataset, we report the average statistical error, the average systematic uncertainty associated with the choice of clean template library, the average amplitude of the off-diagonal terms of the covariance matrix between elements of the sample, the Bessel-corrected average systematic uncertainty and off-diagonal covariance matrix, and the weights given to the three libraries. The top part of the table reports the results obtained by weighting the three clean stellar libraries according to the BIC as described in Section 5. The bottom part of the table reports the results based on equal weights. See text for details.

Sample	$\langle \delta\bar{\sigma}/\bar{\sigma} \rangle$	$\langle \Delta\bar{\sigma}/\bar{\sigma} \rangle$	$\sqrt{\langle C_{i,j}\bar{\sigma}_i\bar{\sigma}_j \rangle_{i \neq j}}$	$\langle \Delta_B\bar{\sigma}/\bar{\sigma} \rangle$	$\sqrt{\langle C_{B,i,j}\bar{\sigma}_i\bar{\sigma}_j \rangle_{i \neq j}}$	Indo-US	XSL	MILES
MUSE-BIC	2.04%	0.21%	0.12%	0.78%	0.45%	0.96	0.04	0
KCWI-BIC	0.86%	0.02%	0.01%	0.67%	0.47%	0.9995	0	0.0005
NIRSpec-BIC	5.73%	0.60%	0.13%	0.85%	0.19%	0.47	0.53	–
SDSS-BIC	3.52%	0.01%	0.01%	1.19%	0.92%	0.00003	0.99997	0
MUSE	2.04%	0.78%	0.47%	0.95%	0.58%	0.333	0.333	0.333
KCWI	0.90%	0.79%	0.70%	0.97%	0.86%	0.333	0.333	0.333
NIRSpec	5.74%	0.60%	0.14%	0.85%	0.19%	0.5	0.5	–
SDSS	3.64%	1.45%	1.30%	1.78%	1.60%	0.333	0.333	0.333

XSL over Indo-US, whereas the opposite is true for MUSE and KCWI. MILES is always disfavored. Our suggested explanation for this difference is that the longer and redder wavelength coverage of the SDSS spectra compared with MUSE and KCWI (3600-5350 Å vs 3600-4500 Å). For example, the Indo-US flux calibration may be better in the blue but less accurate than XSL in the longer and redder wavelength range. The stellar populations that dominate the redder absorption features could also be better described by the XSL library. In contrast, those that dominate in the blue could be better described by Indo-US. This difference highlights the importance of running all the clean stellar libraries.

6.4. General results

We now summarize results that are general and valid across the samples considered here. We also expect them to be valid for

other samples with data of comparable quality. First, once properly cleaned stellar libraries are considered, residual systematics on stellar velocity dispersion due to the template choices are sub-percent. Second, the uncertainty can be further reduced by taking advantage of the information content of the data to select which set of templates better describes the data, according to the procedure described in Section 5. We note that the exact outcome of this process will depend on the data quality and quantity (that set the statistical significance) but also on the wavelength range covered by the data and by the stellar populations in the target galaxies (that may be best described by a specific library or not). Third, the covariance between different galaxies or different spatial bins is also at the sub-percent level. Fourth, there is no single clean stellar library that is preferred by all datasets, so it is important to use all three.

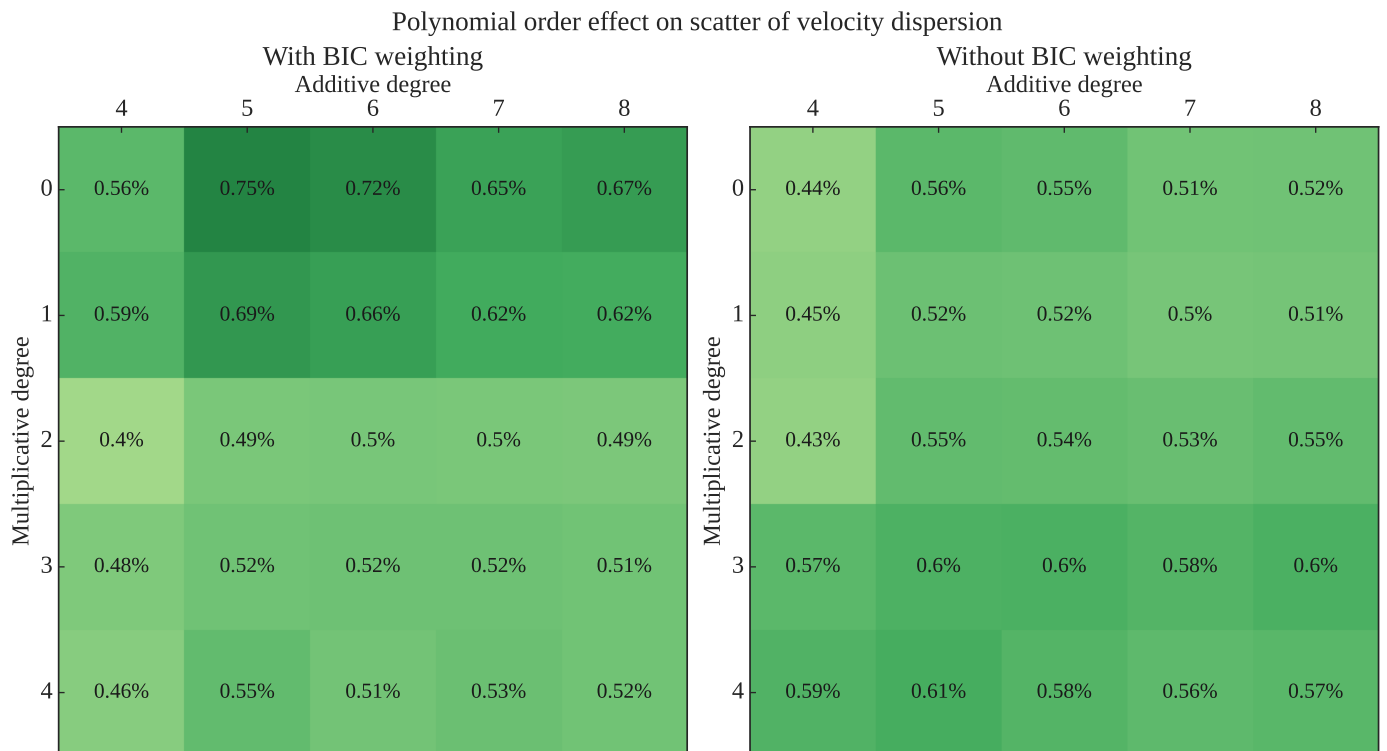


Fig. 16. Average Bessel-corrected systematic scatter of the stellar velocity dispersions for the MUSE sample as a function of polynomial orders, normalized to the weighted average velocity dispersion of the sample. The variations are much smaller than 1%, with and without BIC weighting.

7. Summary

We carried out a detailed study of systematic uncertainties associated with stellar velocity dispersion measurements in samples of massive elliptical galaxies at redshift $z \sim 0.1 - 0.65$. We use spectra with $\text{SNR} \sim 30-160 \text{ \AA}^{-1}$ obtained with three different state-of-the-art instruments, VLT-MUSE, Keck-KCWI, and JWST-NIRSpec. For comparison with previous works, we also study a sample of relatively high SNR spectra from SDSS ($\text{SNR} > 15 \text{ \AA}^{-1}$). We consider three state-of-the-art empirical stellar libraries (Indo-US, MILES, and XSL) as templates. For completeness, we also investigate synthetic libraries that are α enhanced (sMILES) and composite stellar population synthesis (SSP) models that have been used in previous studies.

Our main results can be summarized as follows:

1. For the quality considered here, the main source of systematic uncertainty is the choice of the stellar library to be used as a kinematic template.
2. It is very important to use “clean” stellar libraries, i.e., removing spectra that have defects, such as gaps, poor correction of slit losses, atmospheric absorption and differential diffraction, etc. Not properly cleaned stellar libraries can result in differences of order a few percent and sometimes up to 10-15%.
3. SSP and synthetic α -enhanced libraries can produce results that differ by a few percent with respect to clean stellar libraries, and we discourage their use for high-precision stellar kinematics. For the SSP libraries, we interpret the bias as being due to incomplete coverage of parameter space. This yields insufficient flexibility to reproduce the detailed star formation and chemical enrichment history of massive elliptical galaxies to our desired level of precision. For the α -enhanced libraries, the bias is likely due to known limitations in the modeling of stellar atmospheres (Knowles et al. 2023).

4. Once clean stellar libraries are considered, the residual uncertainty related to the choice of templates is sub-percent for all the primary datasets considered here (MUSE/KCWI/NIRSpec). Even for the lower SNR SDSS spectra they are below 2%. The off-diagonal elements of the covariance matrix between galaxies in a sample and between spatial bins within a galaxy are positive and also sub-percent.
5. We suggest a procedure that uses the Bayes Information Criterion (BIC) to quantify how well each stellar library matches the dataset and assign weights based on the difference in BIC between the stellar libraries. With this optimal weighting, the residual systematic uncertainty and covariance are further reduced to levels well below 1%.
6. The weights of the clean stellar libraries depend on the sample. Our KCWI and MUSE data prefer the clean Indo-US library, while the JWST and SDSS spectra prefer the clean XSL library. It is thus important to make the measurements with all three clean libraries to obtain a complete picture.
7. Other sources of residual uncertainty related to the orders of the polynomials used to model the continuum are shown to be of order 0.2-0.5% for our dataset.

In conclusion, we have shown that adopting the method suggested here leads to a substantial improvement in the precision and accuracy of stellar kinematics measurements, as well as the estimation of the residual uncertainties. While the final precision and accuracy will depend on the properties of the dataset, including wavelength range, the methodology is fully general and can be applied to any dataset. Adopting our procedure enables the standardization and optimization of the measurement of stellar velocity dispersions. This is a crucial step if one wants to use them for cosmography, and will be adopted as standard by the TDCOSMO collaboration.

To facilitate the adoption of our method by third parties, the list of templates and the scripts used in this analysis will be made publicly available after the acceptance of this manuscript through the GitHub repository available at URL https://github.com/TDCOSMO/KINEMATICS_METHODS.

Looking ahead, it is important to note that – When using a measured σ to estimate velocity moments for dynamical models – there are additional sources of potential systematics and model-dependent effects that must be evaluated, mitigated, or corrected, to ensure that 1% accuracy on σ translates to our target of 2% on H_0 . Such considerations include how accurately a Gaussian line-of-sight velocity distribution (LOSVD) approximates the true velocity moment and the corresponding accuracy and precision in mass estimates derived from such models, as well as triaxiality and projection effects (Huang et al. 2025, in preparation). These will be addressed in future papers, building upon the key result of this paper, i.e. the ability to accurately and precisely determine the observable quantity σ .

Acknowledgements. The first two authors should be regarded as joint first authors. We are grateful to S. Trager and A. Vazdekis for sharing with us their quality flags of the XSL and MILES libraries, respectively. We thank A.S. Bolton and M. Bernardi for useful discussions regarding SDSS velocity dispersions. We thank E. Buckley-Geer, M. Millon, and all the friends of the TDCOSMO collaboration for useful feedback that improved this manuscript. This work is based on observations made with the NASA/ESA/CSA James Webb Space Telescope. The data were obtained from the Mikulski Archive for Space Telescopes at the Space Telescope Science Institute, which is operated by the Association of Universities for Research in Astronomy, Inc., under NASA contract NAS 5-03127 for JWST. These observations are associated with program #1974. Some of the data presented herein were obtained at Keck Observatory, which is a private 501(c)3 non-profit organization operated as a scientific partnership among the California Institute of Technology, the University of California, and the National Aeronautics and Space Administration. The Observatory was made possible by the generous financial support of the W. M. Keck Foundation. The authors wish to recognize and acknowledge the very significant cultural role and reverence that the summit of Maunakea has always had within the Native Hawaiian community. We are most fortunate to have the opportunity to conduct observations from this mountain. Based in part on observations collected at the European Southern Observatory data obtained from the ESO Science Archive Facility. Some of the data presented here were taken from the Sloan Digital Sky Survey Archive. Support for this work was provided by NASA through the NASA Hubble Fellowship grant HST-HF2-51492 awarded to AJS by the Space Telescope Science Institute, which is operated by the Association of Universities for Research in Astronomy, Inc., for NASA, under contract NAS5-26555. We acknowledge support by NSF through grants NSF-AST-1906976 and NSF-AST-1836016, and from the Moore Foundation through grant 8548. We acknowledge support from NASA through grants JWST-GO-1974 and JWST-GO-2974. SB thanks the Department of Physics and Astronomy, Stony Brook, for their support.

References

Abdurro'uf, Accetta, K., Aerts, C., et al. 2022, *ApJS*, 259, 35
 Bacon, R., Accardo, M., Adjali, L., et al. 2010, in *Society of Photo-Optical Instrumentation Engineers (SPIE) Conference Series*, Vol. 7735, *Ground-based and Airborne Instrumentation for Astronomy III*, ed. I. S. McLean, S. K. Ramsay, & H. Takami, 773508
 Bacon, R., Accardo, M., Adjali, L., et al. 2010, in *SPIE Conference Series*, Vol. 7735, *Ground-based and Airborne Instrumentation for Astronomy III*, ed. I. S. McLean, S. K. Ramsay, & H. Takami, 8
 Barth, A. J., Ho, L. C., & Sargent, W. L. W. 2002, *The Astronomical Journal*, 124, 2607
 Birrer, S., Millon, M., Sluse, D., et al. 2024, *Space Sci. Rev.*, 220, 48
 Birrer, S. & Treu, T. 2021, *A&A*, 649, A61
 Birrer, S., Treu, T., Rusu, C. E., et al. 2019, *MNRAS*, 484, 4726
 Böker, T., Arribas, S., Lützgendorf, N., et al. 2022, *A&A*, 661, A82
 Bolton, A. S., Burles, S., Koopmans, L. V. E., et al. 2008, *ApJ*, 682, 964
 Bolton, A. S., Burles, S., Koopmans, L. V. E., Treu, T., & Moustakas, L. A. 2006, *ApJ*, 638, 703
 Cappellari, M. 2016, *ARA&A*, 54, 597
 Cappellari, M. 2017, *MNRAS*, 466, 798

Cappellari, M. 2023, *MNRAS*, 526, 3273
 Cappellari, M. & Emsellem, E. 2004, *PASP*, 116, 138
 Chen, G. C. F., Fassnacht, C. D., Suyu, S. H., et al. 2021, *A&A*, 652, A7
 Courteau, S., Cappellari, M., de Jong, R. S., et al. 2014, *Reviews of Modern Physics*, 86, 47
 D'Ago, G., Spiniello, C., Coccatto, L., et al. 2023, *A&A*, 672, A17
 Dressler, A. 1984, *ApJ*, 281, 512
 Dutton, A. A., Brewer, B. J., Marshall, P. J., et al. 2011, *MNRAS*, 417, 1621
 Faber, S. M. & Jackson, R. E. 1976, *ApJ*, 204, 668
 Falcón-Barroso, J., Sánchez-Blázquez, P., Vazdekis, A., et al. 2011, *A&A*, 532, A95
 Jakobsen, P., Ferruit, P., Alves de Oliveira, C., et al. 2022, *A&A*, 661, A80
 Kelson, D. D., Illingworth, G. D., van Dokkum, P. G., & Franx, M. 2000, *ApJ*, 531, 159
 Knabel, S., Treu, T., Cappellari, M., et al. 2024, *arXiv e-prints*, arXiv:2409.10631
 Knowles, A. T., Sansom, A. E., Allende Prieto, C., & Vazdekis, A. 2021, *MNRAS*, 504, 2286
 Knowles, A. T., Sansom, A. E., Vazdekis, A., & Allende Prieto, C. 2023, *MNRAS*, 523, 3450
 Koopmans, L. V. E., Treu, T., Fassnacht, C. D., Blandford, R. D., & Surpi, G. 2003, *ApJ*, 599, 70
 Mamon, G. A. & Łokas, E. L. 2005, *MNRAS*, 363, 705
 Mehrgan, K., Thomas, J., Saglia, R., Parikh, T., & Bender, R. 2023, *ApJ*, 948, 79
 Morrissey, P., Matuszewski, M., Martin, D. C., et al. 2018, *The Astrophysical Journal*, 864, 93
 Sánchez-Blázquez, P., Peletier, R. F., Jiménez-Vicente, J., et al. 2006, *MNRAS*, 371, 703
 Schwarz, G. 1978, *The Annals of Statistics*, 6
 Shajib, A. J., Glazebrook, K., Barone, T., et al. 2022, *The Astrophysical Journal*, 938, 141
 Shajib, A. J., Mozumdar, P., Chen, G. C. F., et al. 2023, *A&A*, 673, A9
 Shajib, A. J., Treu, T., & Agnello, A. 2018, *MNRAS*, 473, 210
 Shu, Y., Bolton, A. S., Brownstein, J. R., et al. 2015, *ApJ*, 803, 71
 Spiniello, C., Tortora, C., D'Ago, G., et al. 2021a, *A&A*, 646, A28
 Spiniello, C., Tortora, C., D'Ago, G., et al. 2021b, *A&A*, 654, A136
 Spiniello, C., Trager, S. C., & Koopmans, L. V. E. 2015, *ApJ*, 803, 87
 Suyu, S. H., Marshall, P. J., Auger, M. W., et al. 2010, *ApJ*, 711, 201
 Treu, T. 2010, *ARA&A*, 48, 87
 Treu, T. & Koopmans, L. V. E. 2002, *ApJ*, 575, 87
 Treu, T. & Marshall, P. J. 2016, *A&A Rev.*, 24, 11
 Treu, T., Stiavelli, M., Møller, P., Casertano, S., & Bertin, G. 2001, *MNRAS*, 326, 221
 Treu, T., Suyu, S. H., & Marshall, P. J. 2022, *Strong lensing time-delay cosmography in the 2020s*
 Valdes, F., Gupta, R., Rose, J. A., Singh, H. P., & Bell, D. J. 2004, *The Astrophysical Journal Supplement Series*, 152, 251
 Vazdekis, A., Koleva, M., Ricciardelli, E., Röck, B., & Falcón-Barroso, J. 2016, *Monthly Notices of the Royal Astronomical Society*, 463, 3409
 Vazdekis, A., Sánchez-Blázquez, P., Falcón-Barroso, J., et al. 2010, *MNRAS*, 404, 1639
 Verro, K., Trager, S. C., Peletier, R. F., et al. 2022, *A&A*, 660, A34
 Verro, K., Trager, S. C., Peletier, R. F., et al. 2022, *Astronomy and Astrophysics*, 661, A50
 Westfall, K. B., Cappellari, M., Bershady, M. A., et al. 2019, *AJ*, 158, 231
 Yıldırım, A., Suyu, S. H., & Halkola, A. 2020, *Monthly Notices of the Royal Astronomical Society*, 493, 4783

¹ Department of Physics and Astronomy, University of California, Los Angeles, CA 90095, USA

² Department of Astronomy & Astrophysics, University of Chicago, Chicago, IL 60637, USA; e-mail: ajshajib@uchicago.edu

³ Kavli Institute for Cosmological Physics, University of Chicago, Chicago, IL 60637, USA

⁴ Sub-Department of Astrophysics, Department of Physics, University of Oxford, Denys Wilkinson Building, Keble Road, Oxford, OX1 3RH, UK

⁵ Department of Physics and Astronomy, Stony Brook University, Stony Brook, NY 11794, USA

Appendix A: Derivation of weighted combination formulae

Here, we provide a derivation of Equations 11, 13, 14, and 16 using variance algebra. We can formulate the problem to solve by first taking a number of random variables X_k with associated weights w_k . Let Y be another random variable that is sampled from X_k with probability $p_k = w_k / \sum_k w_k$. For our use case, X_k is the velocity dispersion distribution from a given template library, and Y is the combined velocity dispersion distribution with weights w_k . Then, the problem is to derive $\mathbb{E}[Y]$ and $\text{Var}(Y)$.

For simplicity, let us denote $\mathbb{E}[X_k] := \mu_k$ and $\text{Var}(X_k) := \sigma_k^2$. Then, we have $\mathbb{E}[Y | K = k] = \mu_k$ and $\text{Var}(Y | K = k) = \sigma_k^2$. From the law of total expectation, we obtain

$$\mathbb{E}[Y] = \mathbb{E}[\mathbb{E}[Y | K]] = \sum_k p_k \mu_k, \quad (\text{A.1})$$

which leads to Equation 11. Similarly, from the law of total variance, we obtain

$$\text{Var}(Y) = \mathbb{E}[\text{Var}(Y | K)] + \text{Var}(\mathbb{E}[Y | K]), \quad (\text{A.2})$$

Here, the first term on the right-hand side above is the *unexplained variance*, which we call the statistical uncertainty, and the second term is the *explained variance*, which we refer to as the systematic uncertainty. The unexplained variance can be expressed as

$$\mathbb{E}[\text{Var}(Y | K)] = \sum_k p_k \sigma_k^2, \quad (\text{A.3})$$

which leads to Equation 13.

To obtain the expression for the explained variance $\text{Var}(\mathbb{E}[Y | K]) := \text{Var}(\mu_k)$, let us first define

$$s^2 \equiv \sum_k p_k \left(\mu_k - \sum_j p_j \mu_j \right)^2. \quad (\text{A.4})$$

Then, the expected value of s^2 is

$$\begin{aligned} \mathbb{E}[s^2] &= \mathbb{E} \left[\sum_k p_k \left(\mu_k^2 + \sum_{i,j} p_i p_j \mu_i \mu_j - 2 \sum_j p_j \mu_j \mu_k \right) \right] \\ &= \sum_k p_k \left(\mathbb{E}[\mu_k^2] + \sum_{i,j} p_i p_j \mathbb{E}[\mu_i \mu_j] - 2 \sum_j p_j \mathbb{E}[\mu_j \mu_k] \right) \\ &= \sum_k p_k \left\{ \text{Var}(\mu_k) + \mathbb{E}[\mu_k]^2 \right. \\ &\quad \left. + \sum_{i,j} p_i p_j (\text{Var}(\mu_i) \delta_{i,j} + \mathbb{E}[\mu_i] \mathbb{E}[\mu_j]) \right. \\ &\quad \left. - 2 \sum_j p_j (\text{Var}(\mu_k) \delta_{j,k} + \mathbb{E}[\mu_j] \mathbb{E}[\mu_k]) \right\} \\ &= \sum_k p_k \left\{ \text{Var}(\mu_k) + \mathbb{E}[\mu_k]^2 \right. \\ &\quad \left. + \text{Var}(\mu_k) \sum_j p_j^2 + \mathbb{E}[\mu_k]^2 \sum_{i,j} p_i p_j \right. \\ &\quad \left. - 2 p_k \text{Var}(\mu_k) - 2 \mathbb{E}[\mu_k]^2 \sum_j p_j \right\} \\ &= \text{Var}(\mu_k) \sum_k p_k \left(1 + \sum_j p_j^2 - 2 p_k \right) = \text{Var}(\mu_k) \left(1 - \sum_k p_k^2 \right). \end{aligned} \quad (\text{A.5})$$

Here, we have used the relation $\sum_k p_k = 1$, which is true by definition. Therefore, an *unbiased* estimate (i.e., with the Bessel correction applied) of the explained variance is obtained by

$$\text{Var}(\mathbb{E}[Y | K]) = \frac{s^2}{1 - \sum_k p_k^2} = \frac{\sum_k w_k (\mu_k - \mathbb{E}[\mu_k])^2}{\sum_k w_k - \sum_k w_k^2 / \sum_k w_k}, \quad (\text{A.6})$$

which leads to Equation 14. Equation 16 can also be derived following the same procedure.